UNIVERSIDADE DE SÃO PAULO
INSTITUTO DE FÍSICA DE SÃO CARLOS

Felipe Pereira Alves

NMR studies on mechanically oscillating samples under magnetic field gradients

São Carlos

2023

Felipe Pereira Alves

NMR studies on mechanically oscillating samples under magnetic field gradients

Dissertation presented to the Graduate Program in Physics at the Instituto de Física de São Carlos da Universidade de São Paulo, to obtain the degree of Master in Science.

Concentration area: Theoretical and Experimental Physics

Advisor: Prof. Dr. Tito José Bonagamba

Corrected version

(Original version available on the Program Unit)

São Carlos

2023

Alves, Felipe Pereira
NMR studies on mechanically oscillating samples under magnetic field gradients / Felipe Pereira Alves; advisor Tito José Bonagamba - corrected version -- São Carlos 2023.
69 p.

Dissertation (Master's degree - Graduate Program in Theoretical and Experimental Physics) -- Instituto de Física de São Carlos, Universidade de São Paulo - Brasil , 2023.

1. Nuclear magnetic resonance. 2. Porous media. 3. Relaxation. 4. Petrophysics. 5. Logging while drilling. I. Bonagamba, Tito José, advisor. II. Title.

This work is dedicated to those I love.

ACKNOWLEDGEMENTS

Em proêmio, nada seria possível sem o apoio dos meus pais, avós, tios, primos, irmão e aqueles que tornam-se família ao longo da nossa jornada. Ao meu irmão, em especial, agradeço por ser uma fonte constante de inspiração através dos seus questionamentos sinceros e profundos, sua busca por clareza e seus desejos por completeza, que estão presentes no meu dia-dia e nas entrelinhas dos meus trabalhos.

Agradeço ao Programa de Pós-Graduação em Física do IFSC/USP pela oportunidade do desenvolvimento deste trabalho e pela excelente formação, bem como aos seus servidores. Em particular, ao Ricardeus, que sempre resolveu as burocracias com celeridade e gentileza. Este trabalho foi desenvolvido em um período histórico no qual as instituições públicas, em especial, de pesquisa merecem, mais do que nunca, serem exaltadas. Estendo o meu agradecimento à população brasileira que mantém as instituições e agências de pesquisa pública do país.

Ao orientador, Tito J. Bonagamba, agradeço a oportunidade de participar do seu grupo, o qual coordena com grande entusiasmo, através de um projeto que integra Academia-Indústria. Agradeço também a todos os membros do laboratório LEAR com quem tive a oportunidade de trabalhar: Aparecido Donizeti Fernandes de Amorim, Edson Luiz Gea Vidoto, Adriane Consuelo da Silva Leal, Arthur Gustavo de Araujo Ferreira, Éverton Lucas de Oliveira, Agide Gimenez Marassi, Ruan Felipe de Oliveira Neves, João Rafael Florentino Silva, Nataly Melo Campos, Edgar Salgado Silva, João Octavio Kül, Davi Gonçalves Sellin, Ygor de Castro Lourenço. Estendo o meu agradecimento ao Willian Andrighetto Trevizan do CENPES/Petrobras pela contribuição no sucesso do projeto.

É impossível a conclusão de um trabalho de pesquisa sem a ajuda de vários amigos. *"É junto dos bão que a gente fica mió"*. Aos meus amigos, escrevo a frase não escrita por Guimarães Rosa para expressar como me sinto: melhor por estar ao lado de pessoas tão boas.

- Agradeço a todos os amigos que conheci em São Carlos. Cada um de vocês contribuiu para tornar essa jornada única e inesquecível. Obrigado por terem me proporcionado momentos de alegria e amizade sincera que serão sempre lembrados com carinho.
- Aos amigos do *Apartamento 61*, com vocês tive a chance de dividir alegrias, muitas horas de café, perrengues e, claro, nas horas vagas, física. Cito com carinho: Felipe *Piconho*, Gabriel *Coxinha*, Fiusa *4K,* Otto *Tricampeão*, Giuliano *Padre*, Léo *Chegado* e *Gustavão*.

- Aos meus alunos de monitoria, que se tornaram amigos, agradeço pelas excelentes experiências, conversas leves, muito bandejão e por me apresentarem a *Tropical Lanches*, que se tornou a minha lanchonete favorita.

- Incluo também neste grupo de amigos, Fernando F. Paiva e Diogo O. Soares-Pinto. Vocês foram fundamentais para uma das etapas que julgo ser essencial para a formação de qualquer pessoa: o seu início. Como mentores nos meus estudos, desempenharam *a arte de ser desnecessário*; e, como amigos, *a arte de ser necessário*. Em ambos os casos, acreditaram em mim.

- Aos meus amigos de João Pessoa, agradeço por sempre me lembrarem o quão bom é estar em Casa. Em especial, vocês foram essenciais para a finalização de parte deste trabalho.

- Agradeço aos inúmeros colegas e membros do grupo LEAR por estimular discussões e colaborações, que estão refletidas neste trabalho. Em especial, por terem dedicado seu tempo e conhecimento para contribuir com as suas correções, fundamentais para melhorar a qualidade e clareza do texto.

Aos servidores da Biblioteca IFSC/USP, agradeço pelo excelente serviço que prestam, sempre com carinho e celeridade. Em especial, a Cris por sua ajuda no processo de correção deste trabalho. Seis anos de formação nesta instituição foram possíveis graças ao notável comprometimento e dedicação de vocês. Além disso, antecipadamente agradeço aos membros da banca por se disporem a avaliar o trabalho, cuja avaliação será de suma importância para o sucesso do projeto.

This study was financed by the Centro de Pesquisa e Desenvolvimento Leopoldo Américo Miguez de Mello (CENPES/Petrobras, 2020/00010-0). We extend our heartfelt gratitude to the funding agencies CAPES, CNPq, and FAPESP, whose unwavering support and investment have been fundamental to LEAR group.

"(...) A vida é breve, a alma é vasta:
Ter é tardar. (...)"
Fernando Pessoa, no livro *Mensagem*

ABSTRACT

ALVES, F.P. **NMR studies on mechanically oscillating samples under magnetic field gradients**. 2023. 69p. Dissertation (Master in Science) - Instituto de Física de São Carlos, Universidade de São Paulo, São Carlos, 2023.

Logging While Drilling (LWD) operations take place within highly complex and demanding environments. This work is an introduction to some of the complex range of phenomena resulting from the combined effects of the Nuclear Magnetic Resonance (NMR) technique, relaxation, diffusion and porous media, with a particular focus on their applications in LWD conditions. Its aim is threefold. First, extracting information from porous media structure requires the development of theoretical models that connect its physical features to the NMR signal. In this regard, theoretical studies were conducted to describe the standard theory behind NMR relaxation and diffusion in porous media. Second, proper interpretation of experimental results remains challenging, in part due to the ill-posed inverse problem related to estimating some parameters from the NMR measurements. In this sense, we have applied the Tikhonov regularization method for parameter estimation. Third, single-sided magnets as a structure probe, in particular, allow one to simulate a petrophysics environment within the laboratory. In this respect, from an experimental perspective, preliminary measurements of a standard liquid were performed to determine the transverse relaxation time (T_2) distributions probed by a benchtop single-sided NMR system, with well-logging tool characteristics: a cylindrical sweet spot with 4 cm of diameter and length; magnetic field of 47 mT centered at 11 cm from the magnet's surface; and a constant gradient of 35.7 G/cm along z. To mimic the operation of an LWD tool, but under standard pressure and temperature conditions, we have established a controlled environment with a mechanical system capable of performing a sinusoidal motion between the sample and the external magnetic field. Our aim is to gain a deeper understanding of the complex patterns within the NMR signal in these scenarios by uncovering their underlying origins and drawing attention to potential caveats associated with the conventional interpretation of NMR relaxation data. Finally, in conclusion, ongoing research is under developing to address extreme conditions that push the frontiers of standard NMR theory, potentially aiding to industrial applications.

Keywords: Nuclear magnetic resonance. Porous media. NMR relaxation. Petrophysics. Logging while drilling.

RESUMO

ALVES, F.P. **Estudos de RMN em amostras mecanicamente oscilante sob gradientes de campo magnético**. 2023. 69p. Dissertação (Mestrado em Ciências) - Instituto de Física de São Carlos, Universidade de São Paulo, São Carlos, 2023.

Operações de *Logging While Drilling* (LWD) ocorrem em ambientes altamente complexos e exigentes. Este trabalho é uma introdução a alguns dos complexos fenômenos resultantes dos efeitos combinados de relaxação, difusão e meios porosos via Ressonância Magnética Nuclear (RMN), com foco particular em suas aplicações em condições de LWD. Seu objetivo é triplo. Primeiro, extrair informações da estrutura de meios porosos requer o desenvolvimento de modelos teóricos que conectem suas características físicas ao sinal de RMN. A respeito disso, estudos teóricos foram conduzidos para descrever a teoria padrão de relaxação e difusão em meios porosos via RMN. Segundo, a interpretação adequada dos resultados experimentais permanece um desafio, em parte devido ao problema inverso mal posto relacionado à estimação de alguns parâmetros a partir das medidas de RMN. Nesse sentido, aplicou-se o método de regularização de Tikhonov para a estimação de parâmetros. Terceiro, magnetos *single-sided*, em particular, permitem simular um ambiente petrofísico no laboratório. À vista disso, de uma perspectiva experimental, medições preliminares de um líquido padrão foram realizadas para determinar as distribuições de tempo de relaxação transversal (T_2) com o emprego de um magneto *single-sided*, com características de ferramenta de perfilagem de poço: um *sweet spot* cilíndrico com 4 cm de diâmetro e comprimento; campo magnético de 47 mT centrado em 11 cm da superfície do ímã; e um gradiente constante de 35.7 G/cm ao longo de z. Para replicar a operação de uma ferramenta LWD, mas sob condições padrão de pressão e temperatura, estabelecemos um ambiente controlado com um sistema mecânico capaz de realizar movimentos senoidais entre a amostra e o campo magnético externo. O objetivo é obter uma compreensão mais profunda dos padrões complexos de sinais RMN nesses cenários, revelando suas origens subjacentes e destacando possíveis ressalvas associadas à interpretação convencional dos dados de relaxação via RMN. Finalmente, em conclusão, pesquisas estão em desenvolvimento para abordar condições extremas que exploram as fronteiras da teoria padrão de RMN, potencialmente auxiliando nas aplicações industriais.

Palavras-chave: Ressonância magnética nuclear. Meios porosos. Relaxometria. Petrofísica. *Logging while drilling.*

LIST OF FIGURES

Figure 1 – Permanent magnets are used in various applications. The range of magnetic field strengths is divided into three categories: intermediate field, low field, and ultra-low field. Low field NMR can be used for relaxation, diffusion, and imaging. Regular permanent magnet technology is used in oil reservoir well-logging and process monitoring, among other applications. Permanent magnet designs are customized for specific purposes and can be open-access or single-sided. 21

Figure 2 – The logging tool's motion varies depending on the conveyance method used. Wireline logging involves a predictable and uniform tool motion, with the cable drawn upwards at a constant rate of around 1.0 m/min in NMR logging. However, wireline tools can experience minor shocks and vibrations when moving through rough boreholes. In contrast, LWD results in a more complex tool motion due to the drilling process introducing axial, rotational, and harmonic motion in all three radial coordinate directions (axial, rotational and lateral). 23

Figure 3 – The figures show the energy level diagrams for spin systems subject to Zeeman interactions. The left panel shows the case for $S = \frac{1}{2}$, while the right panel depicts the situation for $S = 2$. The energy difference between levels is given by $\gamma\hbar B_0$. The bold line represents the expected relative population of the spin states in thermal equilibrium. 26

Figure 4 – The evolution of nuclear spins under the influence of a resonant RF magnetic field can be depicted using a magnetization vector to represent the ensemble of spins. The left figure illustrates this evolution in the laboratory frame, where a longitudinal magnetic field $\mathbf{B}_0$ and a transverse rotating field $\mathbf{B}_1$ are present. When the rotation rate ω_1, relative to the frequency of the rotating field $\mathbf{B}_1$, matches the Larmor frequency $\omega_0 = \gamma B_0$, the magnetization vector simultaneously precesses about $\mathbf{B}_0$ at ω_0 and about $\mathbf{B}_1$ at ω_1. The right figure shows the same system in the rotating frame, where $\mathbf{B}_1$ is stationary. In this frame, the effective longitudinal field at resonance is zero, and only the precession about $\mathbf{B}_1$ is observed. 27

Figure 5 – The T_1 and T_2 relaxation times describe the rate at which the magnetization of a nuclear spin system in a magnetic field returns to its equilibrium value after being perturbed. The relaxation times can be expressed as a function of the correlation time τ_c, which represents the timescale of interactions within the system, at a fixed Larmor frequency ω_0. 29

Figure 6 – A solenoid coil can detect the electromagnetic force (emf) resulting from the precession of the magnetization vector $\mathbf{M}$ at the Larmor frequency $\omega_0 = \gamma B_0$ through Faraday detection. A heterodyne detection scheme is also shown, which involves a combination of independent mixers and low-pass filters assigned to real and imaginary channels. This scheme results in obtaining a complex difference signal $\frac{1}{2}V_0 \exp(-i(\omega_0 - \omega)t)$. 30

Figure 7 – The CPMG pulse sequence produces multiple spin echoes at times $2n\tau$, with each echo being modulated by a T_2 relaxation envelope. 32

Figure 8 – This figure depicts the numerical inverse Laplace transform of a time-domain signal $S(t)$ that decays as a multi-exponential function, along with the corresponding spectrum of relaxation rates, $f(T)$. The regularization parameter α is adjusted to minimize χ^2, as shown by the arrow indicating the chosen value in panel (a). Panels (b) and (c) illustrate $S(t)$ and $f(T)$, respectively, with the latter calculated using a logarithmic spacing of T values. 40

Figure 9 – The experimental setup used for MOS-NMR experiments comprises the following components: (a) a single-sided magnet, (b) a shielded solenoid coil acting as an NMR probe, (c) a series of pulleys that connect to an electric motor driven by a (d) DC power supply to regulate the probe's oscillatory movement, and (e) an oscilloscope used to measure the oscillation frequency. Additionally, an optic sensor is associated with the set of pulleys to synchronize the oscillation to the CPMG experiment. 44

Figure 10 – Schematic illustration for the CPMG pulse sequence in the presence of a static field gradient. 45

Figure 11 – The application of an RF pulse in the presence of a magnetic field gradient results in spatial RF selectivity, exciting only a specific portion of the sample volume. 46

Figure 12 – Visual representation of the accumulated phase resulting from the oscillating motion. Specifically, the accumulated phase Φ is computed as a sum of every phase ϕ leading up to it. 48

Figure 13 – This figure provides a schematic representation of the mechanical oscillation occurring in the presence of magnetic field gradient for a specific case, namely $\theta = 90°$. For more comprehensive information, please refer to the text. 49
Figure 14 – The theoretical model predicts modulation curves that exhibit distinct beating patterns for two conditions: $\theta = 0°$ and $\theta = 90°$. For more details, please refer to the text. 51
Figure 15 – The decay of ^{1}H observed from the CPMG pulse sequence for a bulk sample of Flugel and the corresponding T_2 distribution. 52
Figure 16 – A comparison was made between the experimental data (top images) obtained from CPMG pulse sequences and the modulation curves predicted by the theoretical model (bottom images). The curves were generated for one condition, namely $\theta = 90°$. 54
Figure 17 – Each column displays the NMR signal observed for different oscillation amplitudes along with its respective Inverse Laplace Transform. It is noteworthy that the $T_{2,\text{Select}}$ remains constant across different oscillation amplitudes. However, its contribution increases with the oscillation amplitude. 56
Figure 18 – As we can observe in the experimental results, there are two distinct components in the relaxation process. The faster component has a duration of approximately 0.25 s, which corresponds to half the oscillation period of the sample. This characteristic can be clearly seen in the experimental data. 57
Figure 19 – This figure depicts pulse sequence utilized for diffusion editing, where Hahn echoes are generated in the presence of a static gradient. The first generated echo has an amplitude attenuated by diffusion. 59

CONTENTS

1 INTRODUCTION AND MOTIVATION 19
1.1 Dissertation outline 23

2 NUCLEAR MAGNETIC RESONANCE 25
2.1 Principles of NMR 25
2.1.1 Semi-classical description 25
2.1.2 Signal detection 30
2.1.3 Pulse sequence 32
2.1.3.1 Carr-Purcell-Meiboom-Gill pulse sequence 32
2.1.4 Magnetic field gradients 33
2.2 Relaxation in porous media 34
2.3 Concluding remarks 36

3 NMR SIGNAL PROCESSING AND PARAMETER ESTIMATION . 37
3.1 Motivation 37
3.2 NMR signal processing 37
3.3 Regularization methods 38
3.3.1 Tikhonov regularization 38
3.4 Concluding remarks 40

4 EXPERIMENTAL 43
4.1 Material and methods 43
4.2 CPMG pulse sequence under magnetic field gradients 44
4.3 Spatial RF selectivity 46
4.4 Mechanically-Oscillating-Sample under magnetic field gradients: MOS NMR 47
4.5 Results and discussions 48
4.5.1 CPMG-MOS-NMR decay 48
4.5.2 Spatial RF selectivity effects 52
4.5.3 Moving forward 58
4.6 Concluding remarks 61

5 CONCLUSIONS AND PERSPECTIVES 63

REFERENCES 65

1 INTRODUCTION AND MOTIVATION

Porous media are ubiquitous in Nature. Their structure is relevant to a wide range of both scientific and industrial problems in determining the physical, chemical, and biological properties of the medium.[1–2] In particular, for Petrophysics applications because of the commercial importance of well logging.[3–4] Petrophysics is the study of physical properties of rocks. Since petroleum is found in porous sedimentary rocks, considerable efforts are focused on understanding the relationships between the porous media properties and the fluids that saturate it.[5–7] Nuclear Magnetic Resonance (NMR) techniques are recognized as a powerful method for probing porous media structure and fluid composition.[8–11] Within this context, this work aim to explore, at an introductory level, the following topics.

Porous media. Porous media play an important role in a wide number of disciplines as diverse as petrophysics, biophysics, and chemical engineering. Despite their diversity, ranging from biological tissues to rocks, porous media possess a complex structure at a mesoscopic scale, commonly referred to as the microstructure scale. This structure is of primary interest in numerous applications. An example in Petrophysics applications is rock porosity, essential to assess the oil basin quality.[3–4]

Nuclear Magnetic Resonance. NMR as a structural probe is utilized in a variety of fields such as chemistry, materials science, geology, and biomedicine. Different characterization techniques may be used to obtain useful information on the pore space.[5–7] NMR offers a wide range of methods, and their main advantage is that they are noninvasive and nondestructive, as well as available for in-situ measurements.[8–11]

NMR relaxation and diffusion effects. Spin relaxation and diffusion are key parameters describing the dynamics of the spins under investigation and their interaction with the surrounding environment. In particular, relaxation time analysis is the most common technique used in industrial applications of low-field NMR and is commonly used to characterize fluid type and pore size.[12–13]

NMR parameter estimation. NMR longitudinal relaxation time (T_1), transverse relaxation time (T_2), and self-diffusion coefficient (D) parameters have long been used to characterize porous media. Conventional NMR relaxation and diffusion techniques might extract one of these parameters in a single experiment. In porous media, T_2 provides structural information on the porous material and fluid composition. In particular, it is found to be enhanced by surface relaxation and thus it has been used to measure pore sizes. The distribution of pore sizes leads to a distribution in relaxation rates. Multiexponential relaxation data may be inverted to yield relaxation-time distributions, using the inverse Laplace transform.[14–17]

Petrophysics applications. NMR is recognized by the petrophysical community in the form of well-logging tools. Well logging is the means by which the physical properties of subsurface earth formations are measured in situ. The most important application of well logging is the characterization of hydrocarbon reservoirs: a single-sided permanent magnet and radio frequency resonator are lowered into a well in order to interrogate the fluid properties in the formation near the bore. Once the borehole environment is unusually harsh, this is an immeasurably challenging problem.[3−4,12−13] NMR well-logging was one of the first industrial applications of NMR, starting in the 1950s. Since then, it has become one of the main tools for reservoir profiling and estimation of important properties, such as porosity and permeability. We refer to[18] and the references therein for a historical review.

By necessity, logging tools utilize low-field magnets, since there are significant technical challenges associated with generating a strong magnetic field under the harsh environmental conditions of a well bore. To provide consistent in laboratory measurements, they are designed with permanent magnets (magnetic fields up to $B_0 = 0.05$ T, $\nu_0 = 2$ MHz for ^{1}H) and have become the industry standard in core analysis.[12−13] Low-field NMR plays two significant roles in oil/gas applications: well-logging tools provide access to "reservoir-scale" measurements of the formation fluids, whereas benchtop instruments are used to examine fluids and cored plugs of rock recovered from the reservoir. Interpretations of well logs are supported by laboratory-scale measurements. Benchtop NMR systems provide fluid characterization, rock properties, and a platform for trialing new recovery methods prior to single-well pilots in the reservoir.[11] Figure 1 provides an overview of the prevalent experiments and uses in the field of low-field NMR.

A notable difference between conventional and single-sided magnets is that, in the former, the sample is placed inside the magnet, which represents a limitation, for example, for those larger than the magnet space. Then comes the concept of inside-out NMR, in which, now, the magnet is placed inside the object. When we refer to the study of rock formations, the object is the Earth. The sensitive spot is outside the tool body and has a specific profile within the so-called volume sweet spot. With the use of these magnets and RF coils, it is possible, for example, to study liquids confined in reservoir rocks, although they are not restricted to applications in the oil industry. The reader is referred to[19−20] for a detailed description of single-sided magnets features as well as their extensive application.

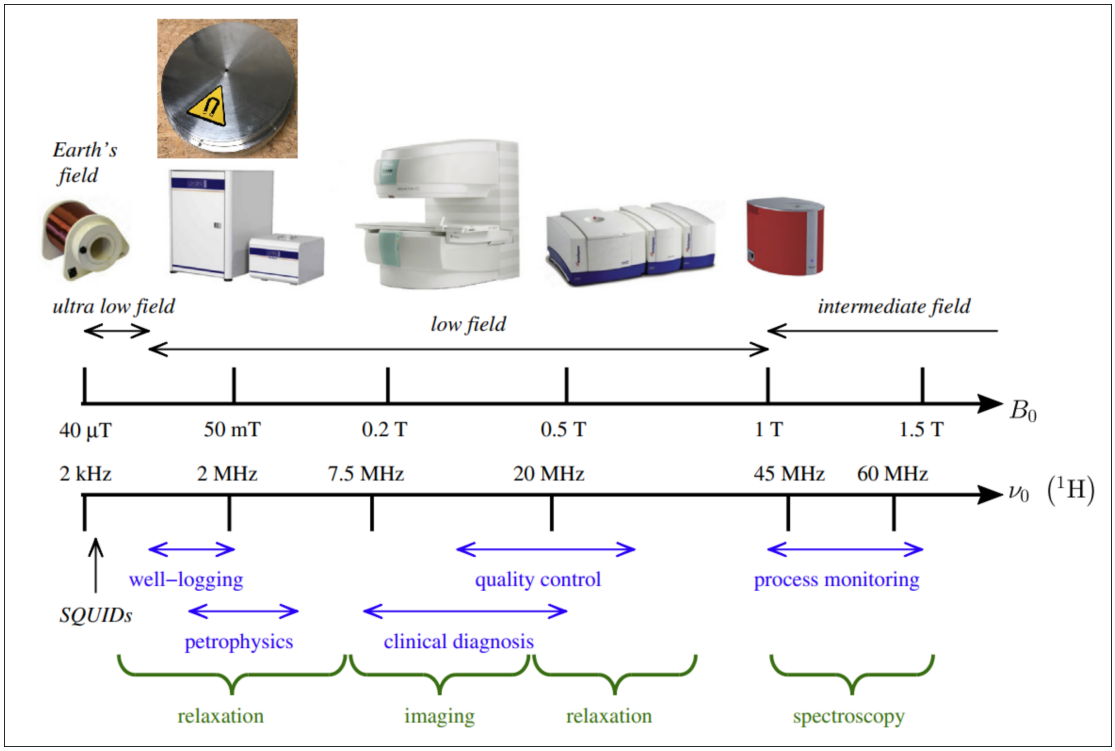

Figure 1 – Permanent magnets are used in various applications. The range of magnetic field strengths is divided into three categories: intermediate field, low field, and ultra-low field. Low field NMR can be used for relaxation, diffusion, and imaging. Regular permanent magnet technology is used in oil reservoir well-logging and process monitoring, among other applications. Permanent magnet designs are customized for specific purposes and can be open-access or single-sided. Source: Adapted from MITCHELL.[13]

The High-Resolution NMR Laboratory (LEAR - IFSC/USP - Brazil) has conducted extensive research using NMR to investigate porous media[21–27] which has contributed to a greater understanding of this subject with potential implications for various industries, as evidenced in the following selected works.[28–40] Currently, LEAR is actively focused on characterizing petroleum reservoirs through the use of unilateral (single-sided) magnets, and has made significant strides in developing novel techniques that employ unilateral NMR instruments to obtain essential reservoir property data.[41–42] In this sense, let's examine the specific issue we are interested in by utilizing unilateral NMR instruments.

Problem. Research in porous media is inherently multi-disciplinary with a broad range of applications.[8] Currently, great efforts are focused on the development of magnets and NMR methods that simulate some reservoir conditions, where some challenges are introduced, such as signal acquisition in the presence of some random movement. To be concrete, this work is part of a research context directly motivated by the understanding of the effects resulting from the logging tools on the NMR signal.[42–46] Figure 2 depicts the tool motions experienced by wireline logging and Logging While Drilling (LWD) tools.

To comprehend the behavior of NMR signals obtained from samples under LWD conditions, but with regular pressure and temperature conditions, it was used a single-sided magnet, probes, and a mechanical system that emulates a relative sinusoidal motion between the sample and the external magnetic field. Specifically, all the developments of this work were performed on a benchtop single-sided NMR system, with well-logging tool characteristics: a cylindrical sweet spot with 4 cm of diameter and length; magnetic field of 47 mT centered at 11 cm from the magnet's surface; and a constant gradient of 35.7 G/cm along z. The reader is encouraged to consult[41–42] for further technical details, as well as preliminary experimental results.

For the remainder of the work, the movements of the LWD tools will be referred to as oscillating movements, as we will limit ourselves to this case. However, it is crucial to note that in practice, this movement is significantly more complex. For instance, while our equipment can replicate the oscillating movements, it cannot fully capture the dynamic and unpredictable nature of the actual drilling process. As such, *any findings and conclusions drawn from our experiments should be interpreted within the context of our experimental setup and may not necessarily reflect the behavior of NMR signals in real-world LWD scenarios.*

Approach to the problem. The focus of this work is specifically on the analysis of a standard liquid data under a very specific set of experimental conditions. We aim to simulate certain LWD conditions through a carefully controlled experimental setup in order to examine the behavior of NMR signals and we will be using the Carr-Purcell-Meiboom-Gill (CPMG) pulse sequence to acquire data. By focusing specifically on the behavior of a standard liquid data under these challenging conditions, we aim to gain a better understanding of the limitations and opportunities presented by NMR in this context.

Expected analysis. In LWD operations, extra signal decay caused by motion-induced factors is a common occurrence. Among these factors, lateral motion is often the dominant source of this decay.[47] The authors in[44] delve into the impact of lateral motion on NMR measurements within the T_2 domain. As lateral-motion can distort the recorded echo train, this may result in a distorted T_2 distribution. Depending on the original T_2 value, this can lead to a shift of a short T_2 peak to shorter values, or the creation of additional peaks in the case of a long T_2 peak. With respect to this matter, based on LWD results and simulated data, they proposed a formula to describe the most complex case, the lateral-motion flow effect.

Goal. The present study represents a significant advancement toward using NMR technology in reservoir characterization despite challenges presented by LWD conditions. The ultimate objective is to improve the accuracy and reliability of NMR-based techniques for measuring fluid properties in complex geological formations under LWD conditions.

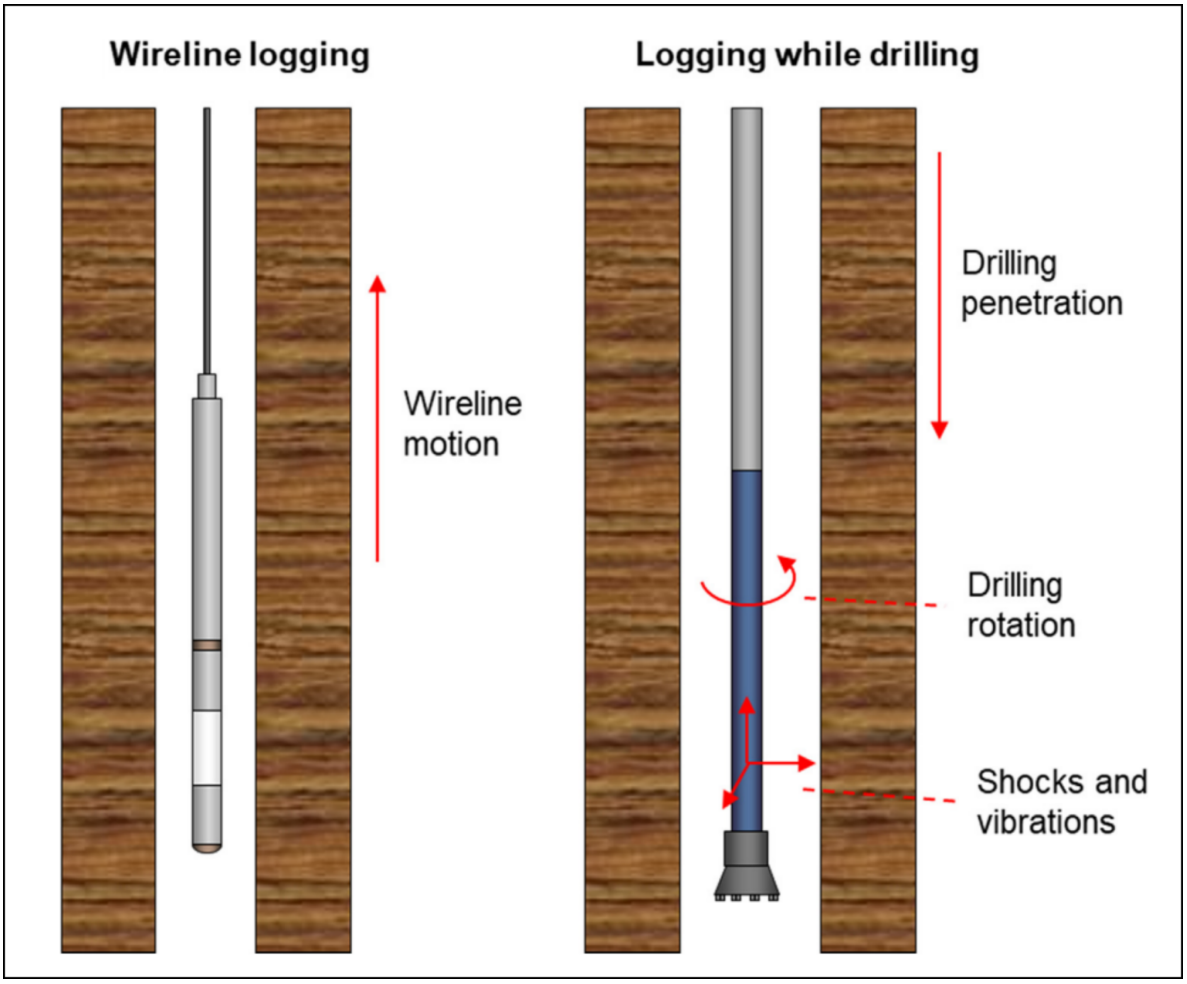

Figure 2 – The logging tool's motion varies depending on the conveyance method used. Wireline logging involves a predictable and uniform tool motion, with the cable drawn upwards at a constant rate of around 1.0 m/min in NMR logging. However, wireline tools can experience minor shocks and vibrations when moving through rough boreholes. In contrast, LWD results in a more complex tool motion due to the drilling process introducing axial, rotational, and harmonic motion in all three radial coordinate directions (axial, rotational and lateral). Source: Adapted from O'NEILL.[45]

1.1 Dissertation outline

Following this brief introduction, the remainder of the dissertation is the result of nineteen months of work (including a global pandemic, coursework, and teacher assistant activities) at the High-Resolution NMR Laboratory (LEAR - IFSC/USP - Brazil). It is organized as follows:

- Chapter 2 introduces fundamental concepts of relevance in NMR, prior to starting the study of methods and techniques to solve problems arising in porous media. In particular, we present the main relaxation mechanisms in porous media.

- Chapter 3 describes the ill-posed inverse problem of finding relevant microstructural features of porous media given the NMR measurements. We introduce the concept of regularization methods to find an adequate solution via inverse Laplace transform. Our attention has been directed towards 1D relaxation experiments.
- Chapter 4 provides preliminary results for the T_2 relaxation parameter estimation performed on a standard liquid probed by a benchtop single-sided NMR system, with well-logging tool characteristics. Herein, we have applied our LWD simulator to mimic the operation of an LWD tool under standard pressure and temperature conditions.
- Chapter 5 concludes by giving a succinct summary of the dissertation's contents, as well as identifying potential avenues for future research.

As we embark on this journey of exploring the fascinating realm of NMR in porous media, it is important to acknowledge the vast array of topics that exist within this field. However, the scope of this work necessitates a focused approach, and thus we have made a deliberate choice to limit our reproduction of content to what we believe is essential for a thorough understanding of the underlying physics at play. It is worth noting that a wealth of information is available in the form of review articles and extensive bibliographies. Interested readers are encouraged to peruse the References section of this work for further reading on these topics.

Moreover, this dissertation serves as a comprehensive and insightful introductory resource for the LEAR group on the complex and intricate topic of NMR in LWD conditions. The extensive literature review, with particular emphasis on the works of[41−42] and the references cited therein, was instrumental in guiding the direction and scope of this study. Therefore, this manuscript can be used as a valuable resource for future investigations on NMR in porous media, in particular, by the LEAR group.

2 NUCLEAR MAGNETIC RESONANCE

NMR explores the interaction of nuclear magnetic moments with magnetic fields. A static field is applied to polarize the sample, time-dependent magnetic RF fields are needed to stimulate the system's response, and magnetic field gradients are used for spatial labeling. This chapter introduces some NMR fundamental concepts in a very synthetic form. Our aim is not to provide full details, rather we have focused on the semi-classical description, which is sufficient for the purposes of this work. For a more complete treatment, as well as the quantum mechanical treatment, we refer to one of many excellent books.[48–50]

2.1 Principles of NMR

2.1.1 Semi-classical description

In 1946, two independent groups, one led by Felix Bloch at Stanford and the other by Edward Purcell at MIT in the US, developed the most widely used method for conducting NMR experiments.[51–52] The detection of changes in nuclear magnetization forms the core of this approach. To accomplish this, the magnetization needs to be perturbed from its initial equilibrium state, where it aligns with the static external magnetic field. Once this perturbation takes place, the magnetization exhibits dynamic behavior. By placing a coil in the plane transverse to the external field, an electromotive force is generated, allowing for the quantification of these dynamics through a macroscopic and observable signal. The pursuit of this signal is the central goal of all NMR experiments.

The fundamental requirement for conducting any NMR experiment is that the sample possesses both a magnetic dipole moment $\boldsymbol{\mu}$, and an intrinsic nuclear angular momentum — nuclear spin $\mathbf{S}$. They are related according to[51]

$$\boldsymbol{\mu} = \gamma \mathbf{S}. \tag{2.1}$$

Here, γ is the gyromagnetic ratio of the nucleus. The gyromagnetic ratio of the proton is $\gamma = 2.675 \cdot 10^8$ T^{-1} s^{-1}. In the presence of electromagnetic fields, the magnetic dipole moments of nuclei interact magnetically with them, for $S = 1/2$; for $S > 1/2$, they interact both magnetically and electrically. Throughout this work, we restrict ourselves to spin-1/2 nuclei that represent most of the experimental works in the field, including the ones presented in this work. The ^{1}H nucleus is probably the most common spin-bearing nuclei among all, especially because of its abundance in biological and mineral samples in the form of water or hydrocarbon molecules. In fact, diffusion experiments probed by ^{129}Xe gas resonance also involve 1/2-spins.[48–50]

To understand any NMR experiment, it is crucial to understand the Zeeman effect — the interaction between the nuclear magnetic dipole moment and magnetic fields (external and local fields) that influence the nucleus. This interaction is responsible for the splitting of different energy levels. The absorption and emission of energy during the transition between these energy levels give rise to the observed phenomenon in an NMR experiment. The following Hamiltonian describes the interaction between a spin $\mathbf{S}$ and a magnetic field $\mathbf{B}_0$[48–50]

$$\mathbf{H} = -\gamma \mathbf{S} \cdot \mathbf{B}_0, \tag{2.2}$$

with eigenvalues

$$E_{\pm} = \mp \gamma \hbar B_0 / 2, \tag{2.3}$$

corresponding to a spin aligned with the field (E_-) or anti-aligned with the field (E_+) (see Fig. 3). For example, protons in a 1 T field yield the energy splitting

$$E_+ - E_- = \gamma \hbar B_0 \sim 10^{-26} \text{ J} \sim 10^{-6} k_B T, \tag{2.4}$$

at room temperature ($T = 300$ K). Thus, a strong magnetic field produces a relatively weak magnetization. In low-field regimes, of the order of mT, this value is even weaker, reduced by 10^{-3} orders of magnitude. More precisely, the small energy splitting is proportional to the external magnetic field and given by Curie's Law[48–50]

$$M_0 = \frac{n \gamma^2 \hbar^2 B_0}{4 k_B T}, \tag{2.5}$$

where n is the density of spin-bearing particles.

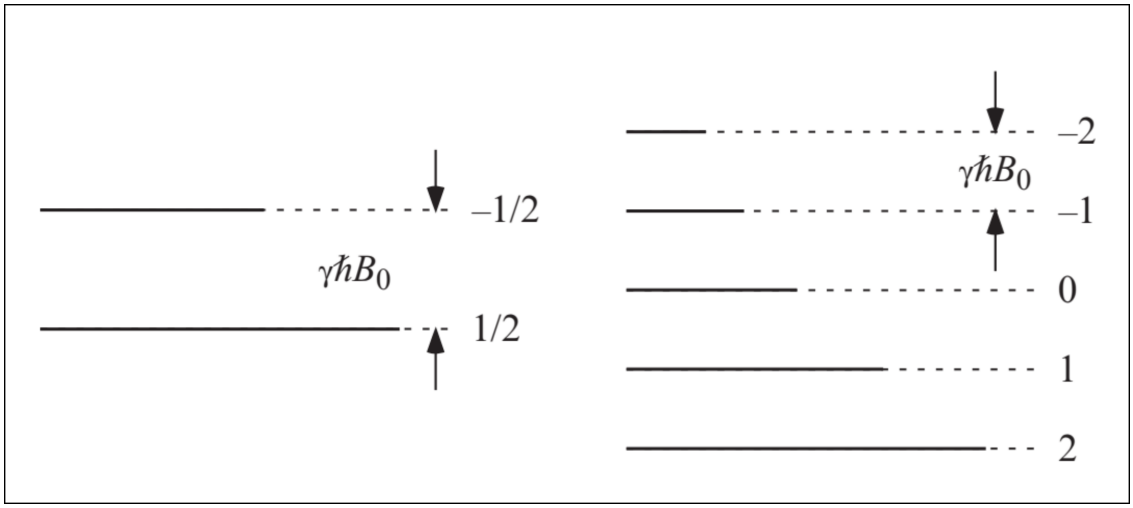

Figure 3 – The figures show the energy level diagrams for spin systems subject to Zeeman interactions. The left panel shows the case for $S = \frac{1}{2}$, while the right panel depicts the situation for $S = 2$. The energy difference between levels is given by $\gamma \hbar B_0$. The bold line represents the expected relative population of the spin states in thermal equilibrium.
Source: Adapted from CALLAGHAN.[53]

Felix Bloch[51] put forward a concise set of equations to describe the time evolution of magnetization based on phenomenological arguments. These equations are often used in NMR, where magnetization is treated as a vector quantity within the semiclassical framework. However, the limitations of this model are evident for systems with $S > 1/2$, necessitating the use of quantum mechanics. Despite these limitations, Bloch's equations remain a valuable tool in the study of magnetization dynamics. The underlying arguments of these equations are explained below.

1. In an arbitrary homogeneous external magnetic field, $\mathbf{B}$, the equation of motion of nuclear magnetization, $\mathbf{M}$, of an ensemble of non-interacting isochromatic spins (in phase) is given by

$$\frac{\mathrm{d}\mathbf{M}}{\mathrm{d}t} = \gamma \mathbf{M} \times \mathbf{B}. \tag{2.6}$$

The above relationship describes a permanent precession movement of the magnetization $\mathbf{M}$ around the field $\mathbf{B}$ for an isolated system when viewed in the laboratory frame (see Fig. 4). The frequency of free precession, for a field $\mathbf{B}_0$, is given by the Larmor relation

$$\boldsymbol{\omega}_0 = -\gamma \mathbf{B}_0. \tag{2.7}$$

For ^{1}H: $\gamma \approx 2.675 \cdot 10^8$ T^{-1} s^{-1} and $\nu_0 = \omega_0/2\pi \approx 42.5$ MHz T^{-1}.

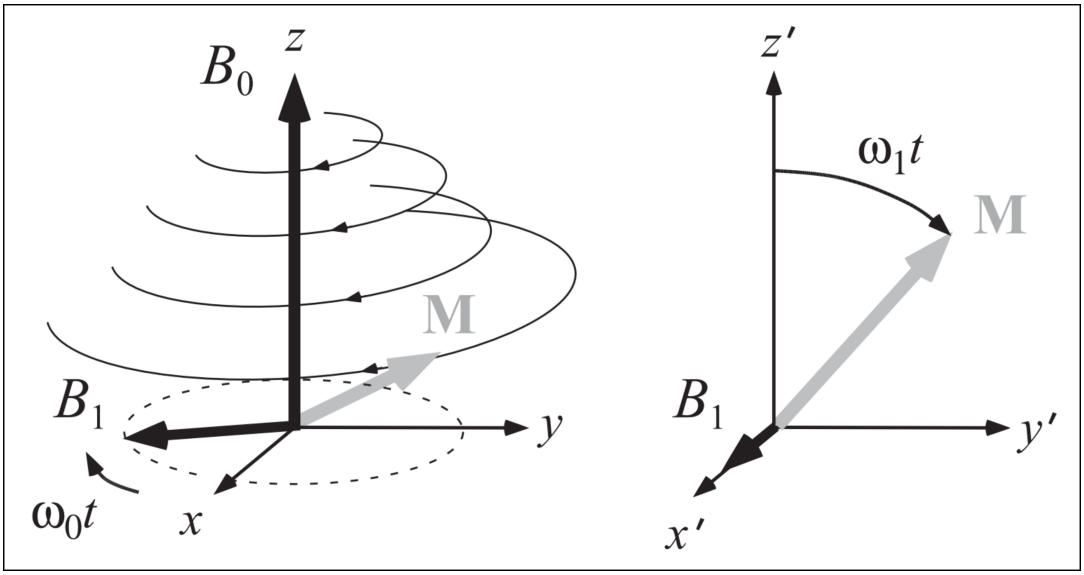

Figure 4 – The evolution of nuclear spins under the influence of a resonant RF magnetic field can be depicted using a magnetization vector to represent the ensemble of spins. The left figure illustrates this evolution in the laboratory frame, where a longitudinal magnetic field $\mathbf{B}_0$ and a transverse rotating field $\mathbf{B}_1$ are present. When the rotation rate ω_1, relative to the frequency of the rotating field $\mathbf{B}_1$, matches the Larmor frequency $\omega_0 = \gamma B_0$, the magnetization vector simultaneously precesses about $\mathbf{B}_0$ at ω_0 and about $\mathbf{B}_1$ at ω_1. The right figure shows the same system in the rotating frame, where $\mathbf{B}_1$ is stationary. In this frame, the effective longitudinal field at resonance is zero, and only the precession about $\mathbf{B}_1$ is observed.
Source: Adapted from CALLAGHAN.[53]

In reality, the system of interest interacts with its environment and neighboring systems. These two types of interactions give rise to what is known as transverse and longitudinal relaxation, which occur simultaneously and independently.[48–50] Bloch developed the concept of transverse and longitudinal relaxation based on the following arguments.

2. When a nuclear spin system is placed in a static field $B_z = B_0$, it reaches a thermal equilibrium magnetization of $M_z = M_0$. However, if the system is disturbed, for instance, by applying an oscillatory radio frequency (RF) pulse $B_1(t)$ perpendicular to the static field, with a frequency ω_1 that meets the resonance condition $\omega_1 = \omega_0$, the magnetization will obtain a component perpendicular to the applied field B_0 (see Figure 4). After turning off the RF field, a transverse relaxation process will occur (it is important to emphasize that the transverse relaxation process is not limited to the period after the RF field is turned off, as relaxation also occurs during the application of subsequents RF pulses). The relaxation process results from the interactions of the nuclear spin system with local fields, which cause a range of different precession frequencies, leading to dephasing. This process progressively reduces the M_x and M_y components of magnetization and can be mathematically described by the following equations

$$\frac{\mathrm{d}M_{x,y}}{\mathrm{d}t} = -\frac{M_{x,y}}{T_2}. \tag{2.8}$$

The solution is given by

$$M_{x,y}(t) = M_{x,y}(0)\exp\left(-t/T_2\right). \tag{2.9}$$

Here, T_2 is the transverse relaxation time. In the laboratory frame of reference, this relaxation process occurs simultaneously with the precession of magnetization around the static field B_0. As a result, Bloch demonstrated that a induced and observable nuclear signal should be detected immediately after the RF pulse is turned off, which can be conveniently measured by a coil positioned in the transverse plane. This signal, referred to as free induction decay (FID), decays with time. This decay is associated with the coherence loss (dephasing due to T_2) during the precession dynamics of the nuclear ensemble.

In practice, there is an additional dephasing (T_2') to T_2, which is determined by the inhomogeneity of B_0 throughout the sample. It is worth noting that the phase loss due to T_2' can be recovered by applying a suitable pulse sequence, whereas the intrinsic delay due to T_2 is not recoverable and is related to random and time-dependent local fields. The combination of T_2 and T_2' provides the T_2^* value given by,

$$\frac{1}{T_2^*} = \frac{1}{T_2} + \frac{1}{T_2'}, \tag{2.10}$$

in the case of macroscopic dephasing be also satisfactorily represented as an exponential decay.[54]

3. During the transverse relaxation process, the longitudinal component of magnetization simultaneously tends to recover its equilibrium value of $M_z = M_0$. This phenomenon occurs due to the interactions between the nucleus and the surrounding medium (lattice). In general, the formulation of this recovery process can be described as follows

$$\frac{\mathrm{d}M_z}{\mathrm{d}t} = -\frac{M_z - M_0}{T_1}. \tag{2.11}$$

The solution is given by

$$M_z(t) = M_z(0)\exp\left(-t/T_1\right) + M_0\left(1 - \exp\left(-t/T_1\right)\right). \tag{2.12}$$

Here, T_1 is called the longitudinal relaxation time.

4. Lastly, it is assumed that the precession and relaxation processes occur independently of each other, leading to Bloch's phenomenological equation

$$\frac{\mathrm{d}\mathbf{M}(t)}{\mathrm{d}t} = \gamma\mathbf{M}\times\mathbf{B} - \frac{1}{T_1}(M_z - M_0)\hat{\mathbf{z}} - \frac{1}{T_2}(M_x\hat{\mathbf{x}} + M_y\hat{\mathbf{y}}). \tag{2.13}$$

The vectors $\hat{\mathbf{x}}$, $\hat{\mathbf{y}}$ and $\hat{\mathbf{z}}$ are the usual Cartesian ones in the laboratory frame of reference.

It is crucial to emphasize that the monoexponential model can only be applied under specific conditions where the interaction terms responsible for transverse relaxation are weak, as described, for example, by the Bloembergen, Purcell, and Pound (BPP) theory.[55] While detailed explanations of the relevant formulas can be found in various sources,[48–50] the monoexponential model is particularly effective in characterizing spins in liquid-state molecules. Figure 5 illustrates the essential features of this model.

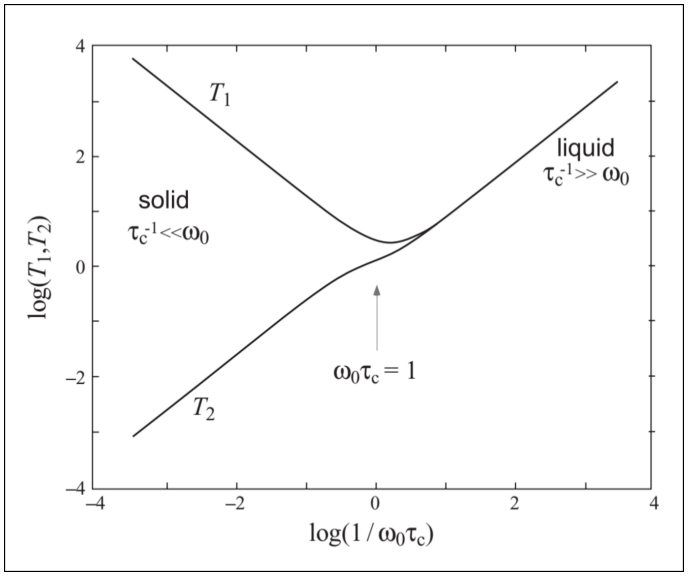

Figure 5 – The T_1 and T_2 relaxation times describe the rate at which the magnetization of a nuclear spin system in a magnetic field returns to its equilibrium value after being perturbed. The relaxation times can be expressed as a function of the correlation time τ_c, which represents the timescale of interactions within the system, at a fixed Larmor frequency ω_0.
Source: Adapted from CALLAGHAN.[53]

However, when dealing with solids and macromolecules that undergo slow motions, the relaxation process becomes more complex, and the monoexponential model may be insufficient to capture this complexity. Nevertheless, since we are limited to observing slowly relaxing spins, the phenomenological approach provided by the monoexponential model remains entirely appropriate in these situations.

2.1.2 Signal detection

Free precession and Faraday detection. The resonant condition of the spins disturbs the magnetization from equilibrium, but what constitutes the NMR signal? The detection of signals in NMR relies on the Larmor precession of non-equilibrium macroscopic nuclear magnetization in the laboratory frame. A coil, such as a solenoid with its axis orthogonal to the z-axis as shown in Figure 6, can detect this free-precession through Faraday induction. The output of the coil is an oscillating voltage.

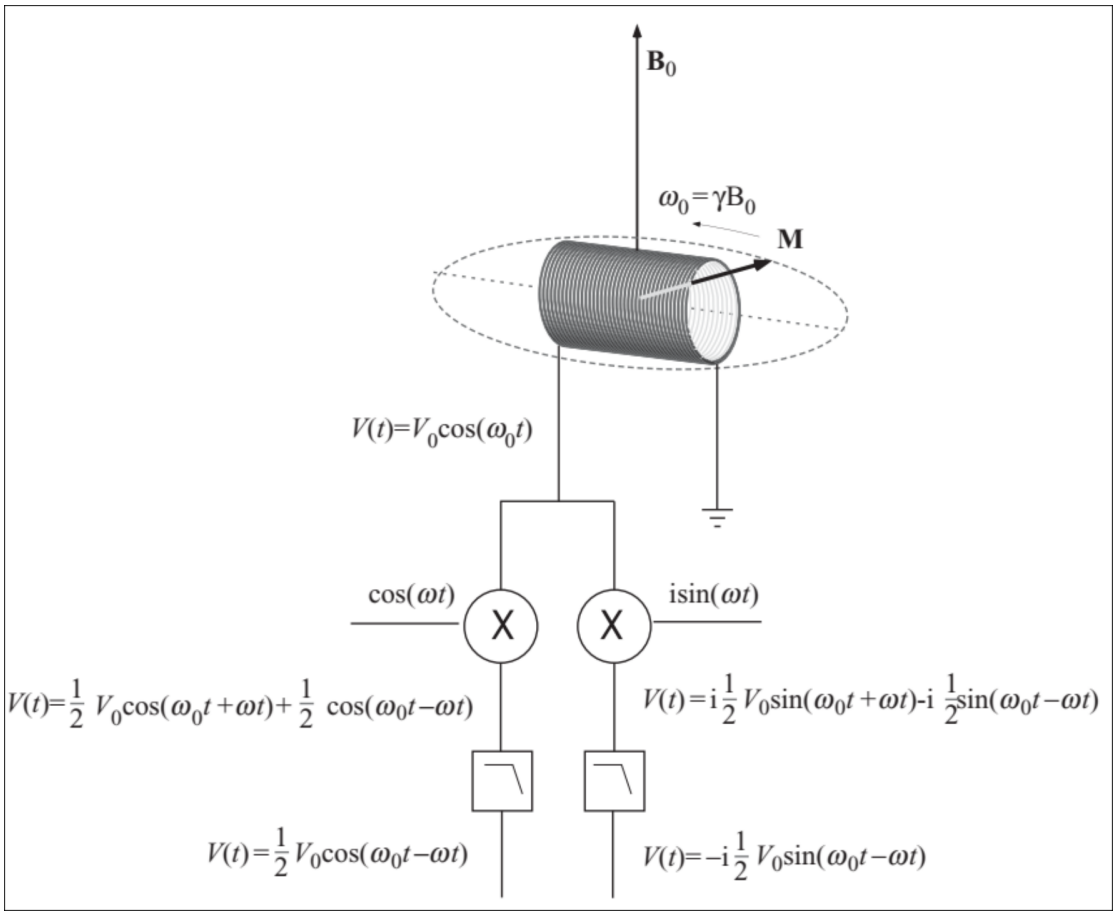

Figure 6 – A solenoid coil can detect the electromagnetic force (emf) resulting from the precession of the magnetization vector $\mathbf{M}$ at the Larmor frequency $\omega_0 = \gamma B_0$ through Faraday detection. A heterodyne detection scheme is also shown, which involves a combination of independent mixers and low-pass filters assigned to real and imaginary channels. This scheme results in obtaining a complex difference signal $\frac{1}{2}V_0 \exp\left(-i\left(\omega_0 - \omega\right)t\right)$.
Source: Adapted from CALLAGHAN.[53]

The specific details of the signal amplitude, which are dependent on factors such as the dimensions of the RF antenna coil, its number of turns, and resistance, are not within the scope of our current discussion. However, one important factor that emerges is that the signal strength will be proportional to the Larmor precession frequency due to Faraday induction. Therefore, high magnetic field strength and large γ are essential for achieving a high sensitivity in NMR signals. Protons are the primary choice for NMR applications due to their large gyromagnetic ratio, high isotopic abundance, and ubiquity in biological tissue, organic molecules, and natural and synthetic materials.

Radiofrequency receivers detect signals by mixing the input signal with a reference RF oscillator, a process known as heterodyning. This detection method is phase-sensitive, meaning that by mixing the signal with two heterodyne references that are 90° out of phase, we obtain separate in-phase and quadrature-phase output signals. These signals are then interpreted as the real and imaginary parts of a complex number. Measurements in reality are always represented by real numbers. Therefore, the separation of the signal into real and imaginary parts requires detection in two independent channels. The actual detection of Larmor precession in a single coil corresponds to a voltage oscillation of the form $V_0 \cos(\omega_0 t)$. By heterodyning with two channels assigned to the real and imaginary parts, we can equivalently represent this as a multiplication of $V_0 \cos(\omega_0 t)$ and $\exp(i\omega t)$ which yields two frequencies, one positive and one negative,

$$V_0 \cos(\omega_0 t) \exp(i\omega t) = \frac{1}{2} V_0 \left[\exp\left(-i\left(\omega_0 - \omega\right) t\right) + \exp\left(i\left(\omega_0 + \omega\right) t\right)\right]. \tag{2.14}$$

The sum frequency term is rejected by the receiver filters and only the difference $\frac{1}{2} V_0 \exp\left(-i\left(\omega_0 - \omega\right) t\right)$ is returned. The negative frequency difference, $(\omega_0 - \omega)$, that is measured is inconsequential, as it only reflects the clockwise nature of the spin precession. The significant aspect is that we can measure $[M_x + iM_y]$ in a frame of reference that rotates at the heterodyne mixing frequency. This enables us to naturally place ourselves in the rotating frame, utilizing it not only for the RF excitation process but also for detection. Henceforth, magnetic resonance phenomena will be discussed from the perspective of the rotating frame as it provides the most natural viewpoint (refer to Figure 4).

It should be noted that when the mixing frequency ω is different from the Larmor frequency ω_0, the signal will oscillate at the offset frequency $\Delta\omega = \omega_0 - \omega$. Therefore, the absolute phase of the heterodyne receiver may not be identical to that of the precessing magnetization, leading to an arbitrary phase factor, $\exp(i\phi)$, in the signal. However, this factor can be removed in the signal processing.[48–50]

2.1.3 Pulse sequence

NMR pulse sequences are used to manipulate and measure the behavior of nuclear spins in a sample. In the context of porous media, the CPMG pulse sequence[56–57] is particularly useful in characterizing the pore size distribution, surface-to-volume ratio, and fluid-solid interactions of porous materials. In conditions similar to LWD, such as in situ measurements, the use of pulse sequences becomes particularly important as the data acquisition is limited by time and space constraints.

2.1.3.1 Carr-Purcell-Meiboom-Gill pulse sequence

The CPMG sequence is one of the most widely used pulse sequences in NMR. To illustrate this method (see Figure 7), let us consider the application of a $\pi/2$ pulse with B_1 along the $+x$-axis at $t = 0$ in the rotating reference frame with frequency ω_1 exactly at the Larmor frequency ω_0. This pulse rotates the magnetization M_0 to lie along the $+y$-axis. At $t = \tau$, if a π pulse is applied with B_1 along the $+x$-axis, an echo is formed at 2τ with the magnetization along the $-y$-axis. By applying another π pulse at $t = 3\tau$, another echo is formed at 4τ, this time along the $+y$-axis. This process is repeated, and successive π pulses at $(2n+1)\tau$ $(n = 0, 1, 2, \ldots)$ form echoes at $(2n+2)\tau$, with the echoes forming along the $-y$-axis for odd n and the $+y$-axis for even n. Since all components of the magnetization in the $x - y$ plane are decaying exponentially with a time constant T_2, which is a result of relaxation processes, the echo sequence also decays exponentially with T_2.

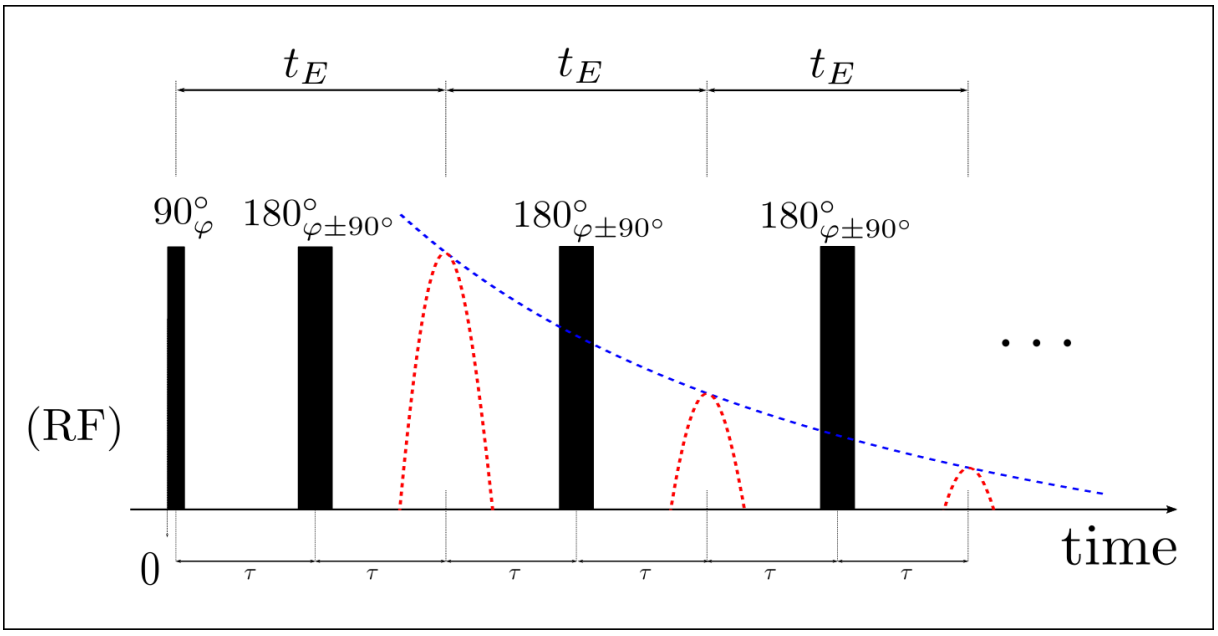

Figure 7 – The CPMG pulse sequence produces multiple spin echoes at times $2n\tau$, with each echo being modulated by a T_2 relaxation envelope.
Source: By the author.

The conventional spin echo method for measuring T_2 requires multiple measurements to be made at different values of τ to obtain the envelope of the echo amplitude as a function of 2τ.[58] However, Carr and Purcell[56] proposed a more convenient method to obtain the entire echo envelope in a single pulse train. This method offers a significant advantage over the conventional spin echo method, as it allows the acquisition of the entire envelope of the echo amplitude in a single measurement.

By recording each Carr-Purcell echo N times, the signal-to-noise ratio is improved by $\sqrt{N}$. However, slight deviations from the π rotation angles in these pulses can lead to cumulative effects that may become significant. To address this, Meiboom and Gill[57] proposed a solution that introduced a 90° phase shift into the radio frequency field between the initial $\pi/2$ pulse and the subsequent π pulses. Therefore, in general, if the B_1 for the $\pi/2$ pulse were oriented along the φ-axis, then the B_1 for the π pulses would be applied along the $\varphi \pm 90°$-axis (refer to Figure 7).

2.1.4 Magnetic field gradients

In our upcoming discussions, we will be introducing a new component that is crucial to understanding the physical system at hand: magnetic field gradients. A magnetic field gradient is responsible for labeling the nucleus by changing their precession frequency according to their position. The simplest and most common choice is a spacial constant gradient, so at a point shifted from the initial position by $\mathbf{r}$, the inhomogeneous magnetic field $\mathbf{B}_G(\mathbf{r}, t)$ varies linearly in space. Hence, we define the local magnetic field as

$$\mathbf{B}(\mathbf{r}, t) = \mathbf{B}_0 + \mathcal{G}(t) \cdot \mathbf{r}, \tag{2.15}$$

with $\mathcal{G}$ being a tensor.[53,59] The equation (2.15) has two contributions: the first one is a strong static magnetic field $\mathbf{B}_0$, responsible for inducing equilibrium magnetization; the second one is a linearly varying field $\mathcal{G}(t) \cdot \mathbf{r}$, responsible for encoding the nucleus by its position. The first affects all the nuclei, in the same way, given by the Larmor frequency $\omega_0 = \gamma B_0$; the second is needed to distinguish the precession frequency from its position.

Under the condition of weak gradients, $|\mathcal{G}(t) \cdot \mathbf{r}| << |B_0|$, the components of the gradient perpendicular to the direction defined by the external field $\mathbf{B}_0$, that we will consider being the z-axis, can be neglected. The remaining components of the gradient tensor, denoted by $\mathbf{g}(t)$, are those parallel to the direction defined by $\mathbf{B}_0$. So, from equation (2.15), the external field takes the form

$$\mathbf{B}_z(\mathbf{r}, t) = \mathbf{B}_0 + \mathbf{g}(t) \cdot \mathbf{r}. \tag{2.16}$$

The equation (2.16), despite providing the necessary spatial distinction for the study of diffusion, does not consider the molecule's stochastic motion, which causes fluctuations in the position $\mathbf{r}$. When the position is treated as a stochastic process $\mathbf{r}(t)$, each nucleus

acquires a random phase $\Phi(\mathbf{r}(t), t)$ due to an inhomogeneous magnetic field, which is obtained by integrating the position-dependent precession frequency along the random trajectory $\mathbf{r}(t)$ of the nucleus,[53,59]

$$\Phi(\mathbf{r}(t), t) = \gamma \int_0^t \mathbf{g}(t') \cdot \mathbf{r}(t') \mathrm{d}t'. \tag{2.17}$$

Equation (2.17) is written in a rotating reference frame with the constant Larmor frequency $\omega_0 = \gamma B_0$, which has no particular interest in the measurement of motion. The random variable $\Phi(\mathbf{r}(t), t)$ is now a functional of the stochastic process $\mathbf{r}(t)$, with initial phase $\Phi(\mathbf{r}, 0) = 0$, which expresses the condition of isochromatic spins (in phase) right after the $\pi/2$ RF-pulse.

Thus, from equation (2.17) each nucleus contributes to the signal attenuation by the factor $e^{i\Phi}$. However, most NMR experiments are performed with a large number of nuclear spins and the detected signal arises not from fluctuations of individual spins but rather from a coherent superposition over all of them. The theoretical approach to this problem is based entirely on the probabilistic interpretation of this superposition. In doing so, the contribution from diffusion to the macroscopic signal can be obtained by averaging the functional $e^{i\Phi}$ over all the nuclei. Since the number of nuclei is very large, the average can be replaced by the expectation over all realizations of the random variable $\mathbf{r}(t)$,[60]

$$E = \langle e^{-i\Phi} \rangle. \tag{2.18}$$

The signal in equation (2.18) is normalized to one in the absence of diffusion-weighting gradient and when no relaxation is present. Note that the signal attenuation due to diffusion in equation (2.18) takes the form of the characteristic function of the random variable phase Φ and leads to an attenuation of the echo due to phase incoherence arising from the random movements of molecules in the system.

It is worth noting that the discussion of magnetic field gradients will be revisited and further elaborated on in the Experimental Chapter of this work.

2.2 Relaxation in porous media

The NMR relaxation times can be particularly useful parameters for porous media characterization since they prove to be sensitive to molecular motion and are affected by the pore geometry.[5–7] In particular, they are extensively used in petrophysical applications to measure porosity and estimate pore size. A complete theory of relaxation involves a myriad of mechanisms that we shall not describe here, rather we focus on the relaxation processes of great interest in porous media. The references should be consulted for a more complete overview.[48–50]

For fluids in porous media, three main independent relaxation mechanisms are involved:

Bulk relaxation. Bulk relaxation, a fluid's inherent relaxation property, is determined by the fluid's physical attributes, including its viscosity and chemical composition. It occurs when a nucleus experiences a magnetic disturbance that oscillates at the Larmor frequency, such as the fluctuation of local magnetic fields from neighboring nuclei's random motion. Bulk relaxation is influenced by environmental factors like temperature and pressure, affecting both T_1 and T_2 relaxation.

Surface relaxation. It has long been known that the NMR relaxation times of fluids in porous media are shorter than in bulk fluids.[5] Diffusion gives a molecule the possibility to collide with nearby solid surfaces, and each collision of a molecule with a surface provides an opportunity for spin relaxation, a phenomenon often called surface relaxation. The problem of surface relaxation for molecules experiencing restricted diffusion in a porous structure was treated in detail by Brownstein and Tarr.[61–62] Independent of the mechanism of surface relaxation, the experimentally measured relaxation rate is often found to be proportional to surface-to-volume ratio (SVR). This mechanism contributes to both T_1 and T_2 relaxation behavior.

Diffusion-induced relaxation. Diffusion in inhomogeneous fields leads to additional attenuation of the CPMG echo amplitudes. When subjected to a CPMG sequence with long inter-echo spacing in a gradient magnetic field, gas, light oil and water exhibit substantial diffusion-induced relaxation. For these fluids, the diffusion-related relaxation time constant becomes a critical parameter for detection. This dephasing is caused by the molecule moving into a region with different magnetic field strength and precession rate and can be mitigated by minimizing the echo spacing t_{E}. The result for the decay term contributed by unrestricted diffusion in the CPMG sequence within the Gaussian approximation is given by[58]

$$\left(\frac{1}{T_2}\right)_D = \frac{1}{12}\gamma^2 G^2 D t_{\mathrm{E}}^2. \tag{2.19}$$

Here, D is the molecular diffusion coefficient, γ is the gyromagnetic ratio of the nucleus, and G is the gradient strength. It's worth noting that diffusion affects only T_2 relaxation and has no impact on the T_1 relaxation rate.

Summary. The relaxation processes act in parallel, and so the rates add

$$\left(\frac{1}{T_2}\right)_{\mathrm{total}} = \left(\frac{1}{T_2}\right)_B + \left(\frac{1}{T_2}\right)_S + \left(\frac{1}{T_2}\right)_D, \tag{2.20}$$

where $(1/T_2)_B$ is the bulk contribution, $(1/T_2)_S$ is the surface contribution, and $(1/T_2)_D$ is the diffusion contribution. The corresponding equation for T_1 is

$$\left(\frac{1}{T_1}\right)_{\mathrm{total}} = \left(\frac{1}{T_1}\right)_B + \left(\frac{1}{T_1}\right)_S. \tag{2.21}$$

Note there is no diffusion contribution to T_1.

2.3 Concluding remarks

To summarize, this chapter covers the key aspects of NMR, including the semi-classical description, the formation of the NMR signal, the application of magnetic field gradients, and the main relaxation mechanisms in porous media. However, it is important to make some brief remarks about how these topics are related to our project.

- Whilst we have presented the concept of gradients in the context of weak gradient regimes, it is important to bear in mind that when it comes to NMR of porous media we may encounter strong magnetic field gradients.[63–64]

  The violation of this regime is less problematic for LWD tools due to gradients originating from the natural non-uniformity of the static field. These gradients can be probed effectively in low-gradient zones. However, LWD tool inhomogeneities may be quadratic in relation to the position relative to the sweet spot. This modification affects the spatial characteristics and acquisition parameter dependence of the spin phase functional, specifically represented by equation (2.17).

In the context of our experiments with liquids in the area of NMR of porous media under LWD conditions, the focus is on bulk relaxation. The decision to neglect the contributions of surface relaxation and diffusion terms in our analysis was made for the following reasons.

- Surface relaxation effects, which are influenced by surface-to-volume ratios, as described by Brownstein and Tarr,[61–62] can be complex. Therefore, although the surface relaxation mechanism is a crucial factor for extracting valuable information about the structure of a porous medium, by neglecting the contributions of surface relaxation, we can simplify our analysis and focus on the more measurable and relevant bulk relaxation parameters.
- Additionally, the diffusion term in NMR relaxation is related to the movement of fluid molecules in the porous media, and can be influenced by factors such as pore size and shape, temperature, and fluid composition. In our experiments, we aim to mitigate the effects of diffusion on our measurements through the use of the CPMG pulse sequence. Specifically, we will use a CPMG pulse sequence with a short echo time.

In summary, while surface relaxation and diffusion effects can certainly be important in certain contexts, in our experiments with liquids in the area of NMR of porous media under LWD conditions, we have chosen to neglect these contributions in order to simplify our analysis.

3 NMR SIGNAL PROCESSING AND PARAMETER ESTIMATION

Inferring microstructure from the macroscopic NMR signal is an intrinsic and formidable inverse problem.[60] Inverse problems are usually characterized by ill-posedness.[65] In order to correctly interpret NMR experiment results and compute the distributions of NMR parameters, it is necessary to process the experimental data with a robust inversion procedure.[15–16,66–67] In this chapter, we will look at an introductory algorithm with the Tikhonov regularization method for NMR parameter estimation. We have focused on 1D relaxation experiments.

3.1 Motivation

The complexity of the physical systems we are interested in does not allow one to access their entire microstructure.[60] Rather, one focuses on estimating some macroscopic parameters sensitive to the local physical environment. As there may be a range of parameters that characterize a given system, usually the NMR parameters investigated are relaxation times (longitudinal T_1 and/or transverse T_2) and self-diffusion coefficient (D). These types of measurements are of special interest in the physics of porous media.

Most experiments in the natural sciences are indirect.[15] That is, the observed data, $S(t)$, are related to the desired function $f(T)$ by

$$S(t) = \int_a^b K(t,T) f(T) \mathrm{d}T + \epsilon(t), \quad c \leq t \leq d. \tag{3.1}$$

Here, $K(t,T)$ is a known kernel, as are the constants a, b, c, d, and $\epsilon(t)$ are unknown noise components, that always exist and have different origins.[14] One is then faced with the standard inverse problem: estimating $f(T)$ from a number of noisy measurements, $S(t)$. Equation (3.1) is a Fredholm integral equation of the first kind and is present in the description of a wide variety of problems. For most of them, estimating $f(T)$ is an ill-posed problem. The concept of ill-posed problems goes back to Hadamard, see for example.[65] In general, the NMR signal describing multiexponential relaxation is described by Fredholm integral equation of the first kind.[16]

3.2 NMR signal processing

In practice, the continuum model of the form given by equation (3.1) needs to be approximated by a discrete model. Write the signal to be inverted, $S(t)$, as a vector arising from the discrete sampling times, t_i, where $i = 1 \ldots N$. The solution $f(T)$ is discretized in the domain of T_j where $j = 1 \ldots M$. If we pre-specify the values of T_j to be used, then we

may calculate a priori $N \times M$ matrix $K_{ij} = K(t_i, T_j)$. Then,

$$S(t_i) = \sum_{j=1}^{M} K(t_i, T_j) f(T_j) + \epsilon(t_i). \tag{3.2}$$

The kernels $K(t_i, T_j)$ are specific for each experiment, describing the expected form of NMR relaxation data. For example, for experiments of the type CPMG, Inversion Recovery (IR), and Saturation Recovery (SR), we have

$$K(t_i, T_j) = \begin{cases} e^{-t_i/T_j}, & \text{CPMG} \\ \left(1 - 2e^{-t_i/T_j}\right), & \text{IR} \\ \left(1 - e^{-t_i/T_j}\right), & \text{SR} \end{cases} \tag{3.3}$$

While in principle $\mathbf{K}^{-1}$ may be calculated algebraically, the matrix $\mathbf{K}$ is "ill-conditioned". This is reflected in the large value of the condition number, defined by the product of the Frobenius norm $\|\mathbf{K}\| \cdot \|\mathbf{K}^{-1}\|$. A large condition number means that the inversion process tends to have an explosive effect on any errors, ϵ_i, in $f(T_j)$. To deal with ill-conditioned, it is necessary to incorporate further information about the desired solution in order to stabilize the problem and to single out a useful and stable solution. This is the purpose of regularization.

To enforce absolute prior knowledge, it is necessary to ensure that all spectral amplitudes are positive, i.e., $f(T_j) > 0$. To incorporate statistical prior knowledge, the solution should aim to minimize the mean-squared residual. In addition, the principle of parsimony dictates that the simplest solution, one that contains only the expected information and the least amount of detail, should be chosen.

3.3 Regularization methods

Having established that many inverse problems are mathematically ill-posed and computationally ill-conditioned, we need to introduce an indispensable technique known as regularization.

3.3.1 Tikhonov regularization

The most well-known and typical method for linear problems is the one known as Tikhonov regularization.[65] As will be shown, it is simple to implement but introduces the classic question: "How can I choose the regularization parameter?".

Here, the idea is as follows: suppose we attempt a least-squares solution $f(T)$ to equation (3.2). Then the sum of squared residuals is

$$\begin{aligned} \chi^2 &= \sum_{i}^{N} \sum_{j}^{M} \left(S_i - K(t_i, T_j) f_j\right)^2 \\ &= \|\mathbf{S} - \mathbf{K}\mathbf{f}\|^2, \end{aligned} \tag{3.4}$$

the quantity we would seek to minimize. Tikhonov regularisation adds a term, $\mathbf{\Gamma f}$, in the minimization process so that the residual to be minimized is

$$\min\left\{\|\mathbf{S}-\mathbf{K}\mathbf{f}\|^2+\alpha\|\mathbf{\Gamma}\mathbf{f}\|^2\right\}, \tag{3.5}$$

where α is known as the regularization parameter. The operator, $\mathbf{\Gamma f}$, is chosen on the basis of parsimony, that is, to favor smoothness with a minimum number of peaks. Commonly used penalties are the square of amplitudes, inclination (first difference), and curvature (second difference). One such smoothness operator might involve the curvature of $f(T)$.

The way to proceed numerically is as follows. We start with the signal vector $\mathbf{S}$, the elements of which, S_i, correspond to each sampling value (for example, time value) labeled t_i, where $i = 1 \ldots N$. Next, we choose a priori range in the solution space of discrete relaxation rates T_j, where $j = 1 \ldots M$. The solution vector $\mathbf{f}$, the distribution of relaxation time, has values corresponding to each T_j and labeled by f_j, with $j = 1 \ldots M$. Thus the solution satisfies

$$\min\left\{\sum_i^N\sum_j^M\left(S_i-K\left(t_i,T_j\right)f_j\right)^2+\alpha\sum_j^M\left(2f_j-f_{j+1}-f_{j-1}\right)^2\right\}, \tag{3.6}$$

where the last term contains the numerical form of the second derivative of $f(T)$. The solution obtained by minimizing equation (3.6) has the least amount of curvature necessary to accurately model the data.

How does one choose the regularization parameter $\alpha > 0$ optimally? This is a difficult question and in general unsolved. One possible method is, after constraining the f_j values to be positive, perform a least squared minimization over a range of α values, and compute the residual in equation (3.4) for each α. We select a value of α that minimizes χ^2 while still adhering to the principle of parsimony.[15−16,66−67]

Therefore, the Tikhonov regularization method is an effective technique for stabilizing the inverse Laplace transform by incorporating a penalty term that discourages significant changes in the T_2 distribution. Furthermore, the non-negativity constraint guarantees that the estimated T_2 distribution is valid from a physical standpoint. An example of time-domain data exhibiting multi-exponential decay with noise, transformed utilizing the Tikhonov regularized least squares, is depicted in Figure 8.

It should be noted that the T_j values can be evenly spaced, but more frequently they are chosen to be equally spaced in logarithmic scale, which allows a broad range of decades to be covered without requiring an extremely large value of M. When running the algorithm, these predetermined T_j values act as “bins” in a histogram that represents the data. As such, they are discrete, and their intensity reflects the total probability of finding the relaxation rate within the range defined by neighboring bins.

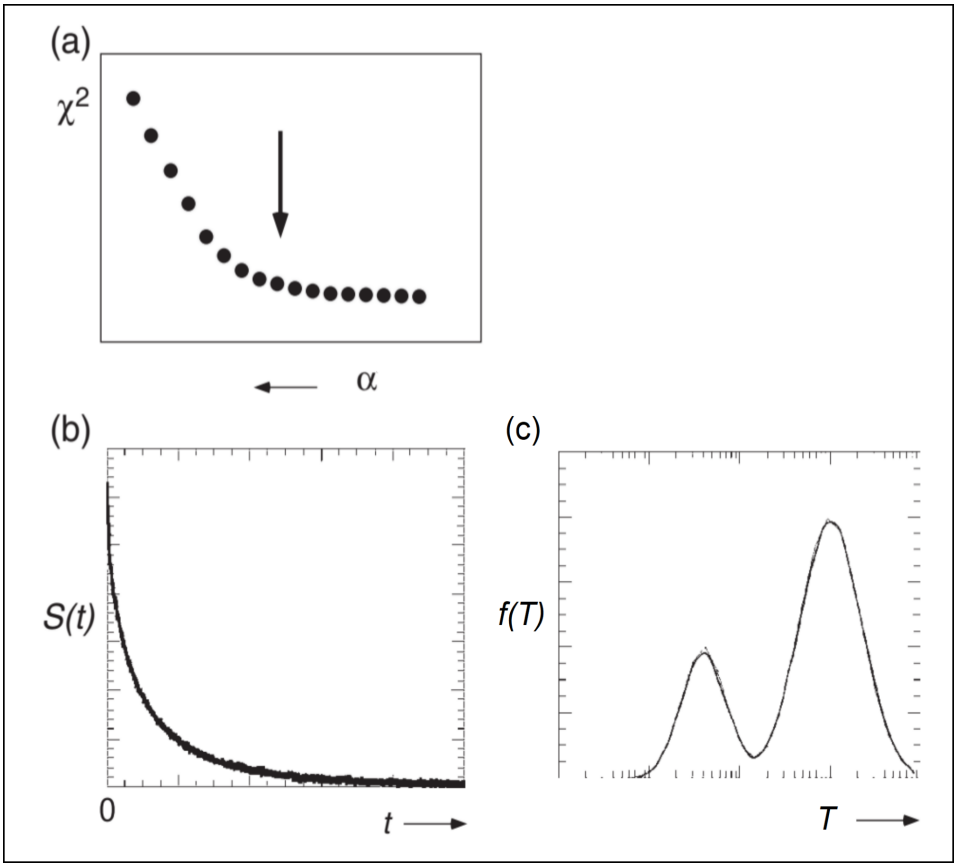

Figure 8 – This figure depicts the numerical inverse Laplace transform of a time-domain signal $S(t)$ that decays as a multi-exponential function, along with the corresponding spectrum of relaxation rates, $f(T)$. The regularization parameter α is adjusted to minimize χ^2, as shown by the arrow indicating the chosen value in panel (a). Panels (b) and (c) illustrate $S(t)$ and $f(T)$, respectively, with the latter calculated using a logarithmic spacing of T values.
Source: Adapted from CALLAGHAN.[53]

3.4 Concluding remarks

Signal processing and parameter estimation play a crucial role in extracting meaningful information from NMR data, particularly in the context of porous media. In order to accurately estimate physical parameters, such as pore size, it is essential to carefully process and analyze the NMR signal. Moreover, regularization methods are essential for overcoming the inherent noise and uncertainty in NMR measurements.

We have presented the basic theory of signal processing and parameter estimation in NMR, along with its fundamental principles and regularization methods, in a succinct yet comprehensive manner. It is important to note how these topics are relevant to our project in the area of NMR of porous media under LWD conditions.

- The Tikhonov regularization method is a powerful tool for signal processing in the field of NMR.[15–16] One of the primary challenges in applying Tikhonov regularization

is selecting an appropriate regularization parameter, which controls the balance between fitting the data and regularizing the solution. If the parameter is chosen inappropriately, it can result in an over- or under-regularized solution.

- While Tikhonov regularization may be a useful starting point, it is important to analyze and study other methods in depth in order to ensure the reliability and accuracy of inversion. In addition to other inversion methods, alternative techniques like the L-curve method or generalized cross-validation can offer more dependable estimates for the regularization parameter. One may find a valuable introductory reading on this topic by referring to[68] and the references therein.

With a deeper understanding of these concepts, we can better apply them to our research on NMR of porous media under LWD conditions.

4 EXPERIMENTAL

Lateral movements of the drilling tool directly affect the NMR measurements, both in its intensity and relaxation rates. To understand the behavior of NMR signals under similar conditions to those of LWD, we have used a single-sided magnet together with a mechanical system that emulates a relative sinusoidal motion between the sample and the external magnetic field. This equipment was used to emulate an LWD tool operating under normal pressure and temperature conditions.[41−42] This chapter presents the main preliminary results from experiments conducted by the author.

4.1 Material and methods

All the developments of this work were performed on a benchtop single-sided NMR system, with well-logging tool characteristics: a cylindrical sweet spot with 4 cm of diameter and length; magnetic field of 47 mT centered at 11 cm from the magnet's surface; and a constant gradient of 35.7 G/cm along z. The experimental apparatus is illustrated in Figure 9.

To carry out the single-sided NMR experiments, a Tecmag NMR console (LapNMR) was utilized in conjunction with a Tomco RF power amplifier (BT00500-AlphaS). An RF solenoid coil was constructed for use with the single-sided magnet. The selected geometry was a solenoid coil, with a length of 50 mm, a diameter of 45 mm, and 34 turns of AWG 19 enameled copper wire wound around a PVC support. This coil can accommodate a cylindrical sample holder with a maximum diameter of 38 mm.

To simulate the oscillating motion in an LWD pattern, the probe was mounted on an acrylic table (refer to Figure 9), which is situated on a platform connected to a set of pulleys linked to an electrical motor (Electro-Craft Servo Products, model M1030) powered by a constant voltage from an external DC power supply (Instrutherm, model FA-3050). The platform, which creates the oscillating pattern, is also connected to an eccentric wheel. An external trigger, linked to a homemade optic sensor and an oscilloscope (Agilent Technologies, model DSO6104A), produces synchronization of the measurements. This fact is important to ensure the acquisition timing of the first measurement from a given initial sample position. At last, the frequency of the oscillation can be regulated by adjusting the voltage applied to the electric motor.

Sample. For the ^{1}H experiments, a 2% (w/v) Sodium-Fluorine Gel (Flugel - DFL) was used. This gel had a neutral pH of approximately 6.5, and its viscosity ranged from 7000-20,000 cP, with a relative density between $0.850 - 1.025$ g/cm^3. The choice of this gel was based on its higher viscosity compared to distilled water. This fact is important

in order to mitigate potential additional effects on the conducted measurements, such as turbulent motions and diffusion effects.

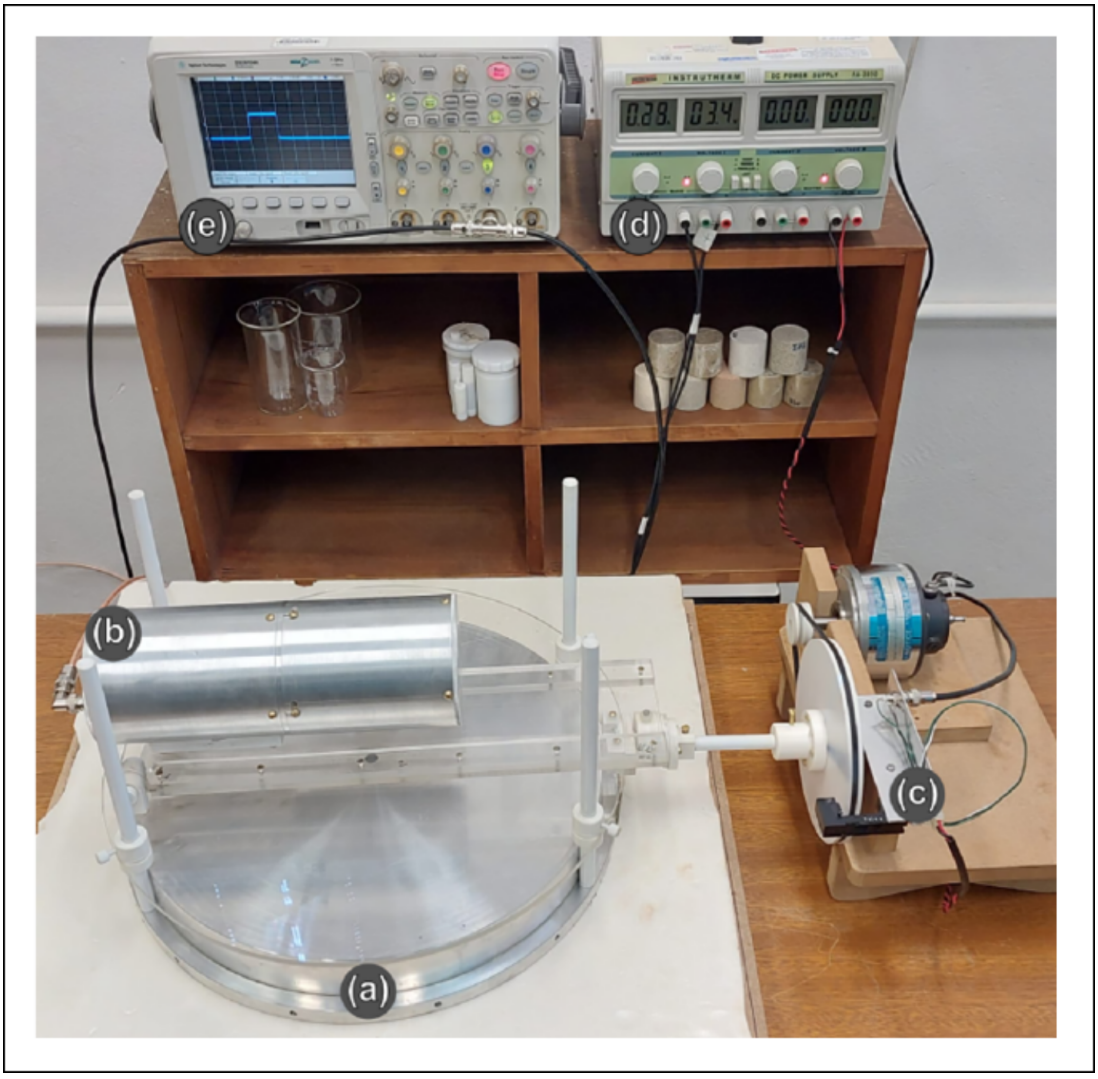

Figure 9 – The experimental setup used for MOS-NMR experiments comprises the following components: (a) a single-sided magnet, (b) a shielded solenoid coil acting as an NMR probe, (c) a series of pulleys that connect to an electric motor driven by a (d) DC power supply to regulate the probe's oscillatory movement, and (e) an oscilloscope used to measure the oscillation frequency. Additionally, an optic sensor is associated with the set of pulleys to synchronize the oscillation to the CPMG experiment.
Source: Adapted from LUCAS-OLIVEIRA.[42]

4.2 CPMG pulse sequence under magnetic field gradients

The CPMG sequence is the primary NMR technique used in the well-logging industry and laboratory sample analysis for evaluating formation and reservoir fluid properties (refer to Figure 7). Similar to the magnetic field gradient used to measure diffusion, static field gradient is also found in specifically designed magnets using permanent

magnetic materials, such as NMR well-logging tool (see Figure 10). The key difference of NMR in the presence of a non-uniform field is the significant off-resonance effect for all pulses, once every pulse is volume-selective (explained in the next section).

Multiple spin echoes at times $2n\tau$ are measured (dashed red line in Figure 10), modulated by a T_2 relaxation envelope (dashed blue line in Figure 10), with n being a natural number. The entire decay curve is acquired during one echo train, so it is possible to determine T_2 in a single experiment, which makes this measurement a very efficient one.

To enhance the signal-to-noise ratio, it is customary to co-add N signals from multiple successive experiments. This approach results in coherent addition of signals, while noise adds randomly, leading to an improved signal-to-noise ratio by $N^{1/2}$.[48–50] Although successive additions can be performed, there is a limitation to the rate at which they can be done. To maintain the nuclear spin system's full signal strength, it needs time to recover its z-axis magnetisation between experiments, which requires a delay of several T_1-relaxation times. This recovery process sets a limit on the number of co-additions that can be performed within a certain time duration.

All the experiments were performed using the standard CPMG acquisition. The widths for the 90° and 180° RF excitation pulses were 10 μs and 20 μs, respectively; echo time t_E = 400 μs; 12.000 sampled echoes; repetition time of 6 s; and 16 averages. The temperatures of the magnet, probes, and samples were kept constant at $(25.0 \pm 0.1)°C$.

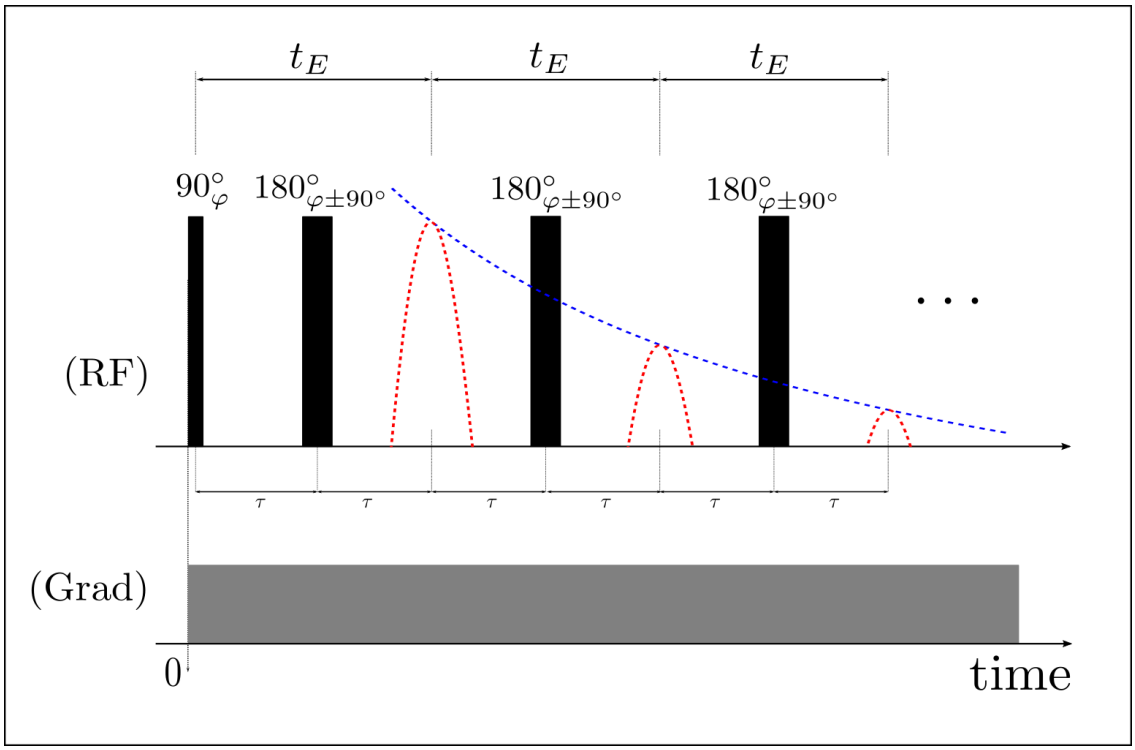

Figure 10 – Schematic illustration for the CPMG pulse sequence in the presence of a static field gradient.
Source: By the author.

4.3 Spatial RF selectivity

The composition of the RF pulses in NMR experiments conducted in the presence of a magnetic field gradient is highly significant as it establishes the effective range of Larmor frequencies that the RF can stimulate, which is defined as a width of $\delta\omega$. The Larmor frequency band can be calculated using the following equation[69]

$$\Delta\omega = \gamma G L. \tag{4.1}$$

One considers the sample length along the G gradient, which is denoted by L. If the value of $\delta\omega$ is less than $\Delta\omega$, then the excitation will be selective and will not stimulate the entirely sample. The excited region will be concentrated in a cross-section that is perpendicular to the gradient direction. The width of this section is given by $\delta L = \frac{\delta\omega}{\gamma G}$. In the case of a rectangular RF pulse, the spectral composition is defined by a sinc function. If the pulse has a duration of t_p, then the predominant excitation band region is defined by the central lobe of this sinc function, which is in the interval $\left[-\frac{1}{t_p}, +\frac{1}{t_p}\right]$.[69] For instance, if a rectangular pulse of duration $t_p = 20$ μs is applied the excitation band is approximately $\delta\omega = 100$ kHz. In the presence of a magnetic field gradient of approximately $G_0 = 35$ Gauss/cm along z, this pulse will excite a cross-section of approximately $\delta L = 7$ mm, as shown in Figure 11.

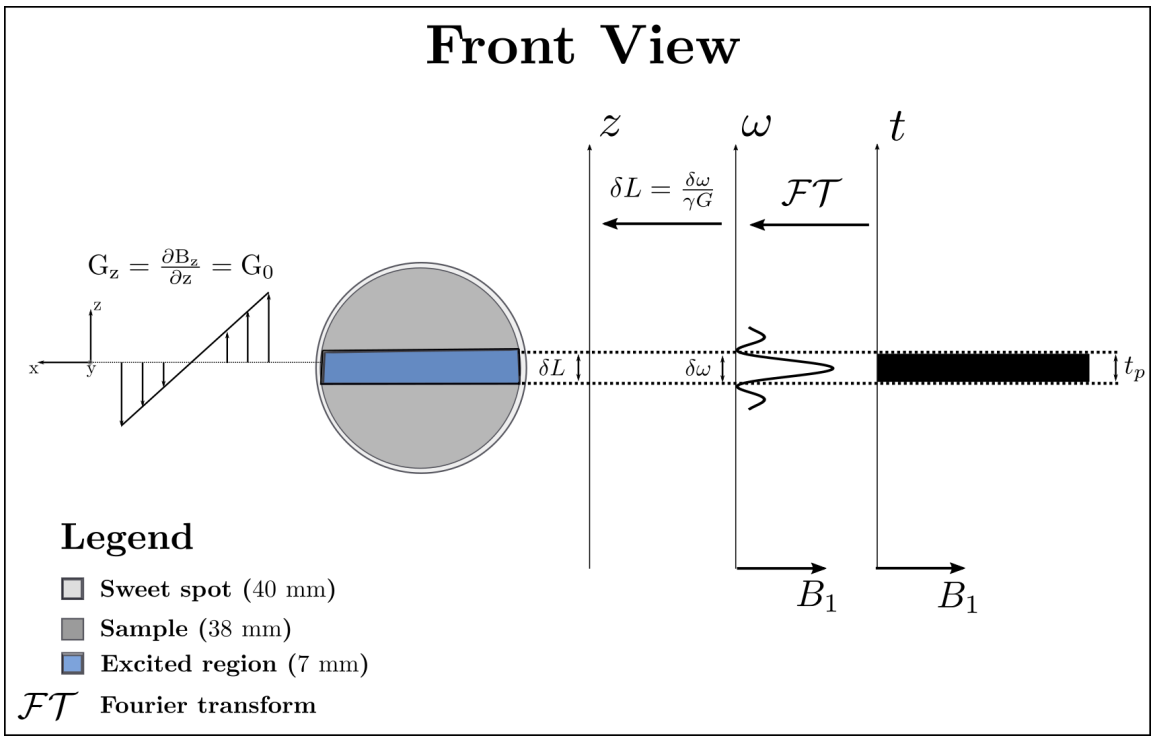

Figure 11 – The application of an RF pulse in the presence of a magnetic field gradient results in spatial RF selectivity, exciting only a specific portion of the sample volume.
Source: By the author.

4.4 Mechanically-Oscillating-Sample under magnetic field gradients: MOS NMR

MOS-NMR experiments are conducted with the sample localized in a region where the magnetic field is given by the expression

$$\mathbf{B}(\mathbf{r}, t) = \mathbf{B}_0 + \mathbf{G} \cdot \mathbf{r}(t). \tag{4.2}$$

In this context, $\mathbf{B}_0 = B_0\hat{\mathbf{z}}$ represents the main external magnetic field; $\mathbf{G} = G_0\hat{\mathbf{z}}$ is the magnetic field gradient across the sample region; and $\mathbf{r}(t)$ denotes the nuclear spin position. Assuming that the sample undergoes a sinusoidal oscillation in time with amplitude a_0 and frequency Ω, and considering the direction of the magnetic field gradient $\hat{\mathbf{z}}$, we have $\hat{\mathbf{z}} \cdot \mathbf{r}(t) = z(t)$. Therefore, the position $z(t)$ can be expressed as follows

$$z(t) = z_0 + a_0 \sin(\Omega t + \theta), \tag{4.3}$$

where θ is a phase that depends on sample initial position.

In the case of a CPMG MOS-NMR experiment, as the spin undergoes sinusoidal motion along the magnetic field gradient, additional accumulated phases arise for each dephasing (ϕ_1) and refocusing (ϕ_2) periods τ around the π pulses, affecting the amplitudes of the signal. This effect can be generalized by considering the phase accumulated between any two intervals $(n-1)\tau$ and $n\tau$. The general phase is given by (refer to Eq. (2.17))

$$\begin{aligned} \phi_n &= \gamma G_0 \int_{(n-1)\tau}^{n\tau} [z_0 + a_0 \sin(\Omega t + \theta)]\, \mathrm{d}t \\ &= \gamma G_0 z_0 \tau + \frac{\gamma G_0 a_0}{\Omega} [\cos(\Omega(n-1)\tau + \theta) - \cos(\Omega n\tau + \theta)]. \end{aligned} \tag{4.4}$$

Here, n is in the range of $[1, 2, 3, \ldots]$. The case of thermal initial conditions will be considered for z_0.

Each echo has an accumulated phase Φ corresponding to the sum of the phases leading up to it, considering the sign changes introduced by the π pulses. Thus, the total accumulated phase is given by (see Figure 12)

$$\Phi_n = \phi_n - \Phi_{n-1}(-1)^n. \tag{4.5}$$

The term $(-1)^n$ accounts for the effect of the π pulse every 2τ intervals.

The CPMG pulse sequence produces observed echoes every interval of $t_E = 2n\tau$. Thus, the NMR signal can be calculated using the following expression

$$\overline{M}(2n\tau) = M(2n\tau) \exp\left(-i\Phi_{2n}\right). \tag{4.6}$$

Here, $\overline{M}$ is the modulated signal caused by the sinusoidal motion of the sample relative to the magnet. It is important to emphasize that the relaxation effects result in a monoexponential decay, as explained in the NMR Chapter. This means that incorporating these effects into our descriptions is relatively straightforward.

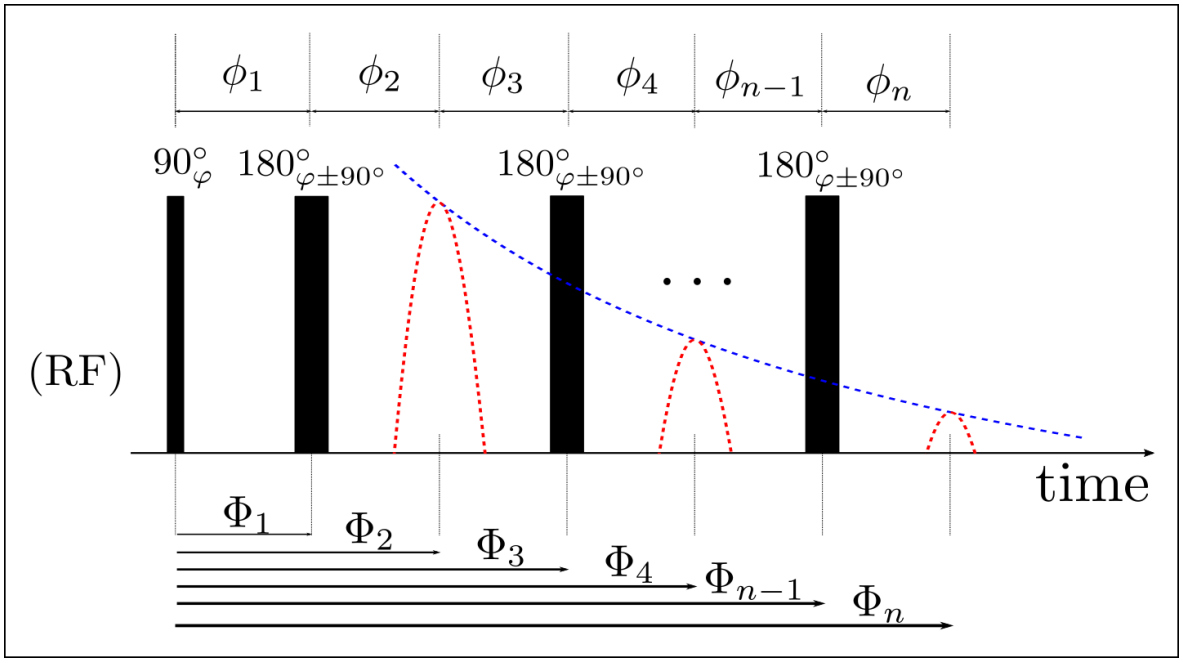

Figure 12 – Visual representation of the accumulated phase resulting from the oscillating motion. Specifically, the accumulated phase Φ is computed as a sum of every phase ϕ leading up to it.
Source: By the author.

4.5 Results and discussions

4.5.1 CPMG-MOS-NMR decay

Theory. Initially, we will focus on presenting the results associated with this theoretical model, which are described by the equations (4.4) - (4.6), to gain some insight into the physics of the problem and the experimental data utilizing the following set of parameters: gyromagnetic ratio of the proton, $\gamma = 2.675 \cdot 10^8$ T^{-1} s^{-1}; constant gradient, $G_0 = 35.7$ G/cm; echo time, $t_E = 400$ μs; mechanical system amplitude, $a_0 = 2$ mm; mechanical system frequency, $\Omega = 2$ Hz; and T_2-relaxation, $T_2 = 1$ s. This last value will be justified in the upcoming section, as it is connected to Flugel's T_2.

In equations (4.4) - (4.6), it is observed that the signal modulation patterns depend on the initial sample position, which is an important point to consider in understanding the experimental results. One can then simulate the magnetization decay under two different initial conditions defined by the angles $\theta = 0^\circ$ and $\theta = 90^\circ$.

Figure 13 presents a diagrammatic illustration of the mechanical oscillation under the influence of a magnetic field gradient, specifically for the case where $\theta = 90^\circ$, which encompasses all the physics of the problem. Although this image is primarily pictorial, it will be frequently employed as a valuable aid in unraveling the complexity of the phenomena involved in our physical system.

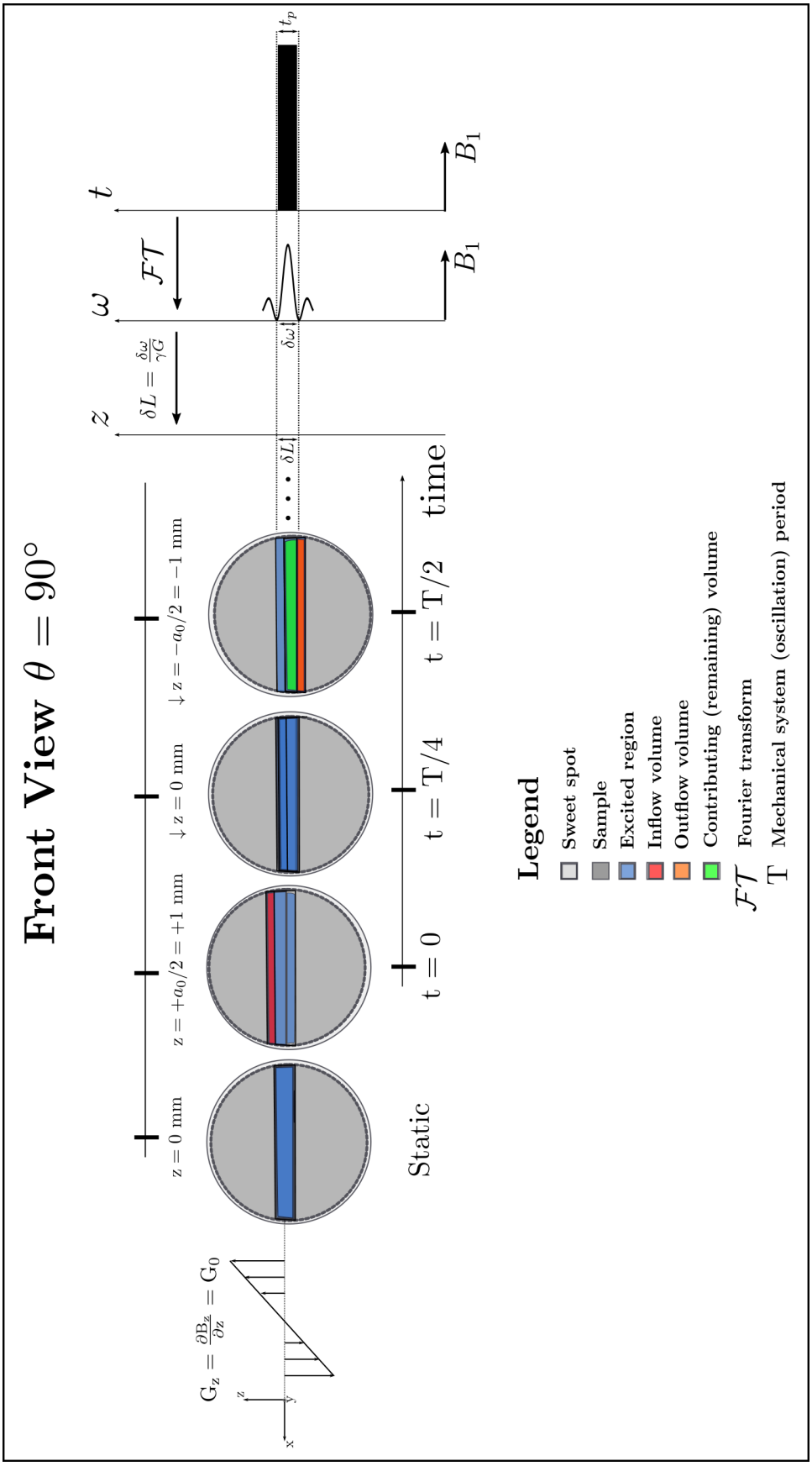

Figure 13 – This figure provides a schematic representation of the mechanical oscillation occurring in the presence of magnetic field gradient for a specific case, namely $\theta = 90°$. For more comprehensive information, please refer to the text.
Source: By the author.

- At t = 0.

    1. The sample is situated at its initial synchronized position, z = $+a_0/2$ = +1 mm.[1]
    2. At this stage, it is important to note that the sample has zero initial velocity.
    3. As a result of the sample's location at its initial synchronized position of z = $a_0/2$ = +1 mm, a portion of the sample volume that will enters the *excited region* (denoted by the blue color) will not have been previously excited, the so-called *inflow volume* (denoted by the red color).

- At t = T/4.

    1. The sample passes through the region with z = 0 mm.
    2. At this stage, the sample presents its maximum velocity.
    3. As the sample passes through the current region with z = 0, the previously *inflow volume* is fully contained within the *excited region*.

- At t = T/2.

    1. The sample reaches the position z = $-a_0/2$ = −1 mm.
    2. At the position of z = $a_0/2$ = −1 mm, a portion of the previously excited volume will now extend beyond the *excited region*, creating an *outflow volume* (denoted by the orange color).

- At t ≥ T/2.

    1. The sample will have reached a *steady state* stage, meaning that the *inflow* and *outflow* sample volume will now have been defined within the *excited region*, resulting in a *contributing (remaining) volume* (denoted by the green color).
    2. This cycle will continue in a similar fashion, with the sample oscillating around its equilibrium position, z = 0 mm, with a oscillation amplitude of a_0 = 2 mm.

With the aid of this visualization, let us now delve into the results obtained from the theoretical model for both cases, $\theta = 0°$ and $\theta = 90°$, which are depicted in Figure 14. All plots presented in this manuscript were generated by the software MATLAB.

[1] It is important to make a significant remark regarding the reference used for measuring the amplitude of oscillation. In Figure 13, we will be presenting the oscillation denoting an amplitude of a_0 = 2 mm between the intervals of [z = $+a_0/2$, z = $-a_0/2$], which differs from the implication of equation (4.3) which suggested [z = $+a_0$, z = 0]. It must be noted that this decision was taken with the sole purpose of better representing the visualization of observed phenomena, without any observable impact on our results — at the current stage of our work — as elucidated by our forthcoming discussion of the results.

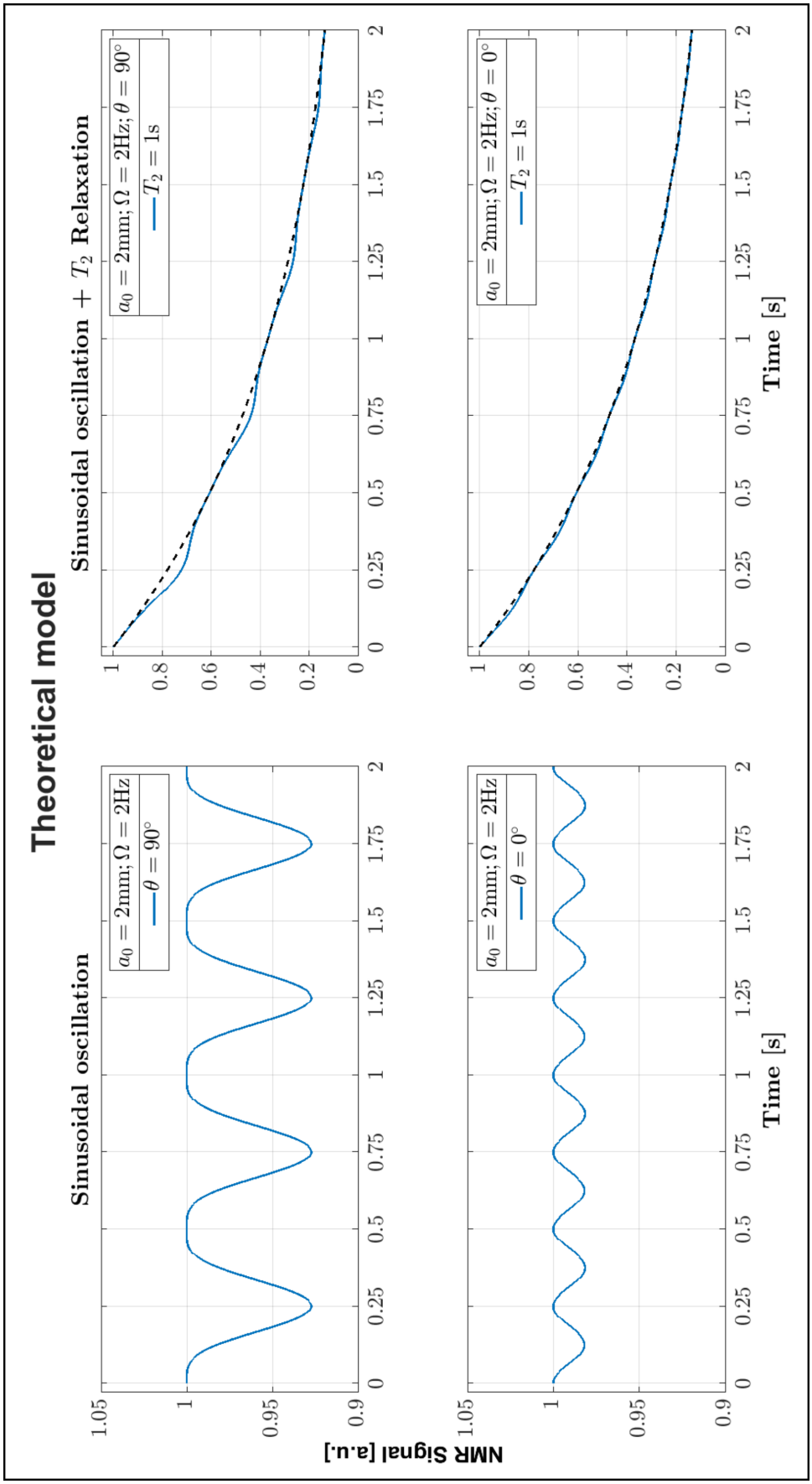

Figure 14 – The theoretical model predicts modulation curves that exhibit distinct beating patterns for two conditions: $\theta = 0°$ and $\theta = 90°$. For more details, please refer to the text.
Source: By the author.

From now on, the dashed black line represents the intrinsic decay of T_2, while the solid blue line is associated with the sinusoidal oscillation. It is important to highlight that the *phase modulation* graphs exclusively reflect the effects of sample oscillation on the NMR signal under the assumption that the entire oscillating volume remains within the *excited region*. This fact has inherent limitations for our physical system as will be seen moving forward to the next discussion, and it is crucial to compare these results with experimental data to further validate their reliability and accuracy.

Moving forward in our analyses, we will focus on the $\theta = 90°$ case as it produces a more visible effect on the NMR signal.

4.5.2 Spatial RF selectivity effects

Experiment. In order to precisely control the frequency, amplitude, and sample position relative to the magnet, the experimental setup was meticulously designed. While the system is simpler than those utilized for reservoir conditions in terms of coil and magnet geometry, it was carefully constructed to achieve optimal performance. A solenoid coil was utilized in the setup, which offered several advantages. Firstly, it allowed for the observation of phase modulation caused by sample movement. Additionally, the uniform RF magnetic field in the sweet spot provided by the solenoid coil allowed for pulse selectivity to be achieved with less complexity.

Figure 15 provides a clear visualization of the signal decay observed through the application of the CPMG pulse sequence, as well as the corresponding T_2 distribution, for the ^{1}H Flugel experiment with a static sample. This figure serves as an essential reference for analyzing the results of the experiment.

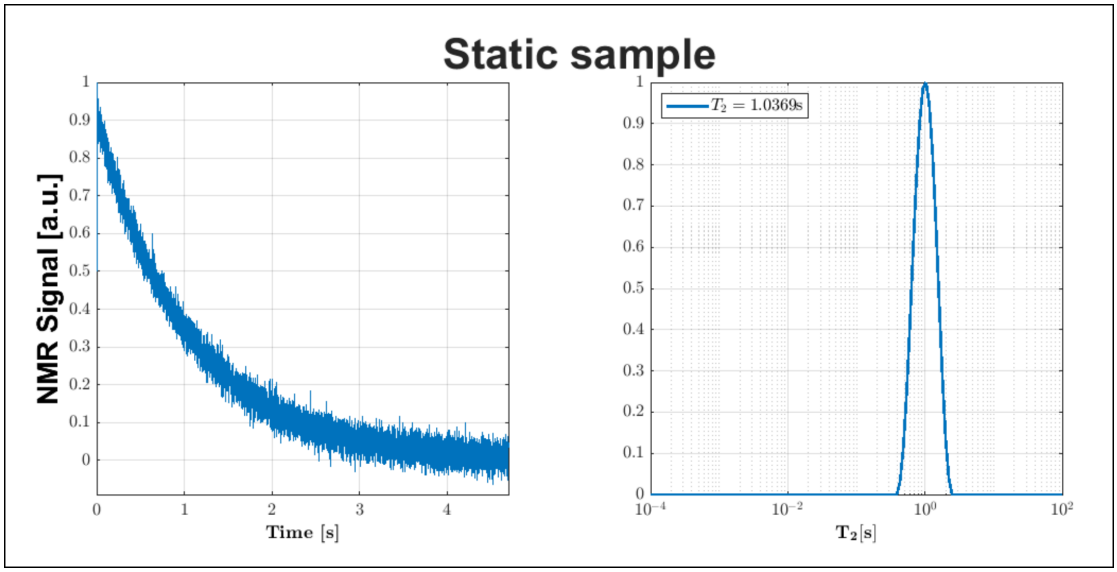

Figure 15 – The decay of ^{1}H observed from the CPMG pulse sequence for a bulk sample of Flugel and the corresponding T_2 distribution.
Source: By the author.

Echo train. One important distinction between signals obtained from uniform magnetic fields and those from high-gradient fields is the difference in the shape of the observed echo. In a uniform magnetic field, the echo is broad enough to be observed over a range of milliseconds, allowing for more points to be acquired before and after the exact CPMG refocusing time. This results in a flatter region around the echo's top, which can increase the signal-to-noise ratio without affecting the average intensity value.

However, the same cannot be said for high-gradient fields, as the narrow shape of the echo leads to a rapid decay of points around the top. Even a slight deviation of tens of microseconds can result in a significant change in magnitude and phase, making it difficult to obtain a higher signal-to-noise ratio. In theory, the observed effects can be explained by focusing on the maximum point of refocusing, which corresponds to the top of the echo. Therefore, utilizing the smallest observation window provides results that are closer to the theoretical values. However, this approach comes at the cost of a significantly lower signal-to-noise ratio, which poses a disadvantage. In all of our experiments, we have utilized an echo window of 50 points and an echo time of 400μs, which was selected specifically to minimize the influence of diffusion effects.

We will now discuss the results obtained for configurations using a fixed frequency of $\Omega = 2$ Hz and different amplitudes $a_0 = [0, 1, 2]$ mm. Our initial focus is to compare these results with our theoretical model. In Figure 16, we present a comparison between the experimental data obtained from CPMG pulse sequences and the modulation curves predicted by our theoretical model.

The theoretical framework examined in this manuscript does not yet incorporate an essential aspect of the phenomenon under study, namely, *spatial RF selectivity* effects. This implies that the model does not account for the potential impact of a reduced excited volume of the sample due to mechanical oscillation (as depicted in Figure 13). This, in turn, can lead to a decrease in the intensity of the NMR signal, as the signal strength is directly proportional to the number of excited particles. As a result, the experimental data obtained from the echo trains exhibit decay rates that surpass the predictions generated by the theoretical model. In particular, refer to Figure 16, looking closely at the oscillation with an amplitude of $a_0 = 2$ mm, since this case has a more visible impact on the NMR signal.

Therefore, our initial analysis suggests that *spatial RF selectivity* effects is a crucial factor that influences the decay rates of echo trains in our physical system. Consequently, it is essential to incorporate this effect in experimental design and interpretation to obtain precise and dependable results. The subsequent analyses of this work will aim to explore and clarify the causes and consequences of it, with the analysis of the T_2 distributions serving as a starting point.

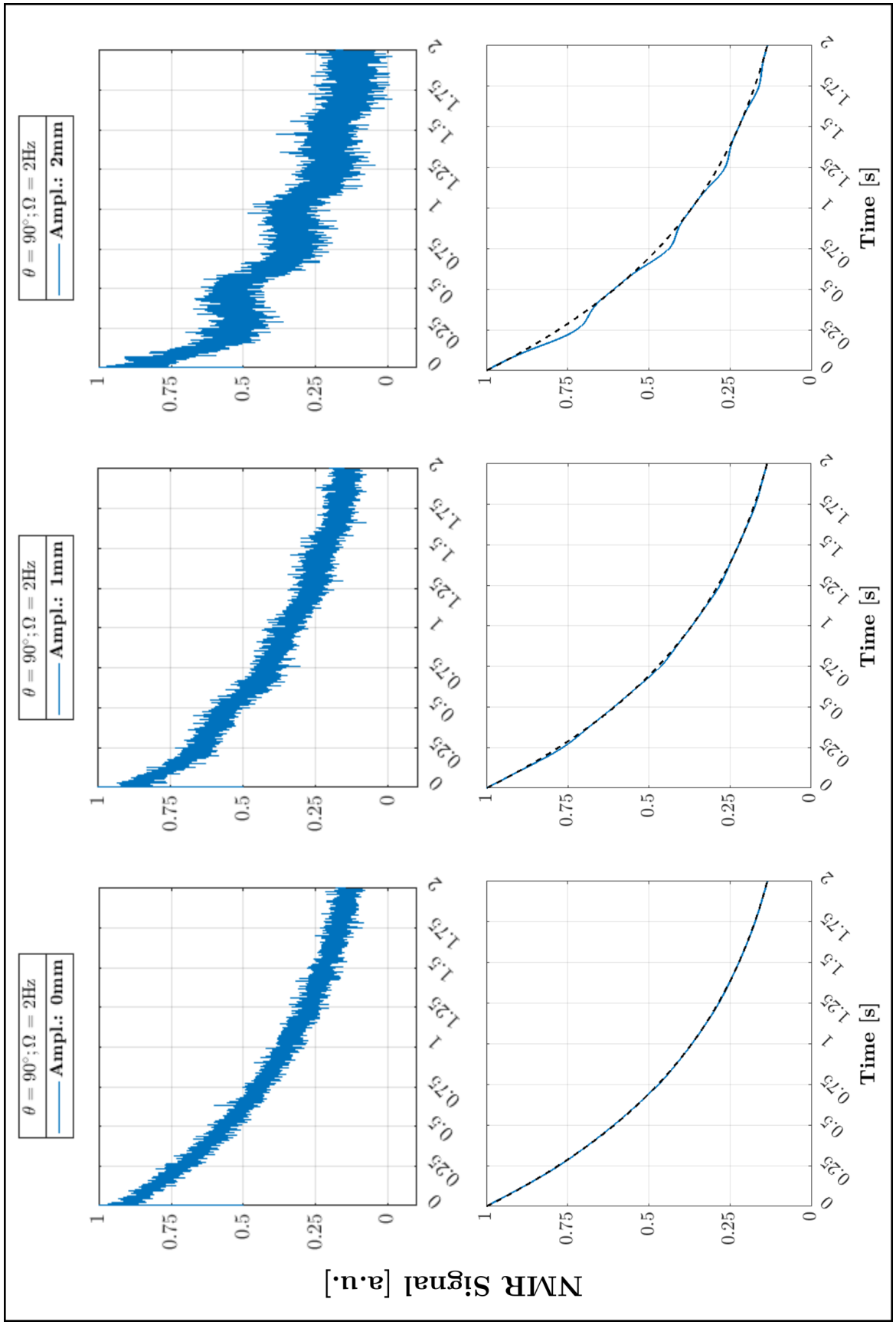

Figure 16 – A comparison was made between the experimental data (top images) obtained from CPMG pulse sequences and the modulation curves predicted by the theoretical model (bottom images). The curves were generated for one condition, namely $\theta = 90°$.
Source: By the author.

T_2 distribution. Let us now shift our focus towards the examination of the T_2 distribution and how it responds to motion. We will be performing a relaxation time analysis on the same data previously discussed. This approach will allow us uncover any additional insights that may further our understanding of the system.

Figure 17 shows the results for a fixed frequency of $\Omega = 2$ Hz and different amplitudes $a_0 = [0, 1, 2]$ mm. Upon closer examination, we observed the presence of *two relaxation times* as the mechanical system amplitude increased. Despite a change in signal amplitude, which varies in intensity depending on the corresponding oscillation amplitude, the relaxation time for each peak remains constant.

The presence of *two relaxation times* in the relaxation process can be further illustrated in Figure 18. Once again, we will be closely examining the case that corresponds to an oscillation with an amplitude of $a_0 = 2$ mm, once this particular case has a more pronounced effect on the NMR signal. The so-called *faster relaxation time* lasts for approximately $\mathrm{t} = 1/2 \cdot \mathrm{T} = 1/2 \cdot 1/\Omega = 0.25$ s, which is half the oscillation period.

The *spatial RF selectivity* effect significantly influences the time evolution of the NMR signal in our physical system, especially during the initial stages of the signal. The experiment was synchronized by $\theta = 90°$ and the sample volume was then displaced in and out from the *excited region* for half of the oscillation period until it reached the *steady state* stage (refer to Figure 13). Based on our findings, we can tentatively conclude that the decay observed in our experiments cannot be entirely explained by the physical relaxation property T_2 alone. Instead, the effects of *spatial RF selectivity* must also be considered. Consequently, the *faster relaxation time* observed can be attributed to the *spatial RF selectivity* effect, which we refer to as $T_{2,\mathrm{Select}}$.[42]

These findings are align with the expected analysis made in the Introduction Chapter that lateral motion can distort the recorded echo train, resulting in a distorted T_2 distribution. In particular, lateral motion can create additional peaks in the case of a long T_2 peak.[44] Therefore, as a partial conclusion, we can infer that the NMR signal can be segregated into two distinct regions based on their characteristics, as shown in Figure 18.

- The first region is where *spatial RF selectivity* effects are predominant and is visible until the *inflow* and *outflow* volumes have been defined within the *excited region* and reach the *steady state* stage, as depicted in Figure 13.
- After this transient period, the NMR signal evolves under the effect of *phase modulation*, which is responsible for the further evolution of the NMR signal in the second region.

It is worth noting that these two regions are experiencing the intrinsic physical decay that is linked to transverse relaxation.

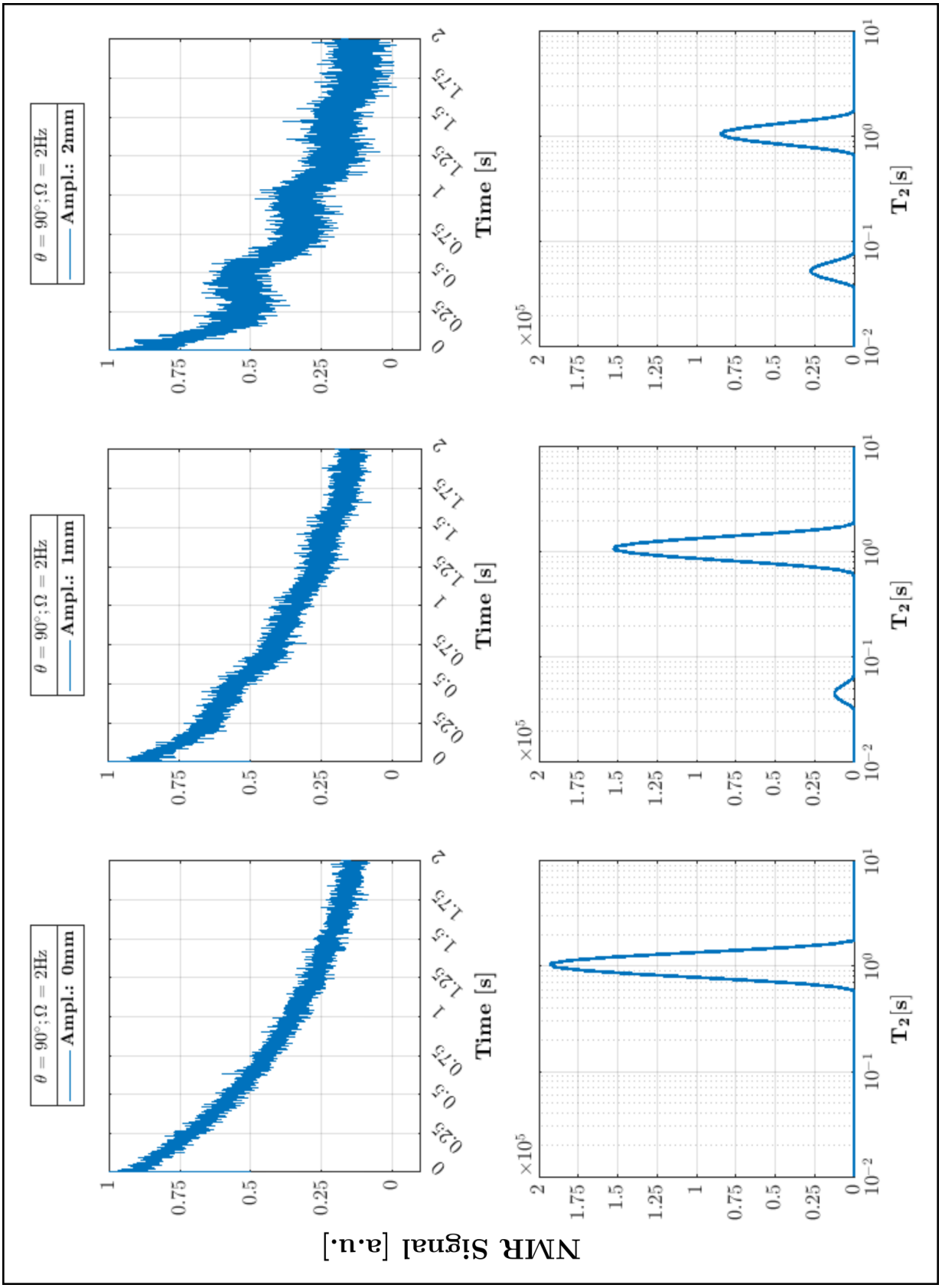

Figure 17 – Each column displays the NMR signal observed for different oscillation amplitudes along with its respective Inverse Laplace Transform. It is noteworthy that the $T_{2,\text{Select}}$ remains constant across different oscillation amplitudes. However, its contribution increases with the oscillation amplitude.
Source: By the author.

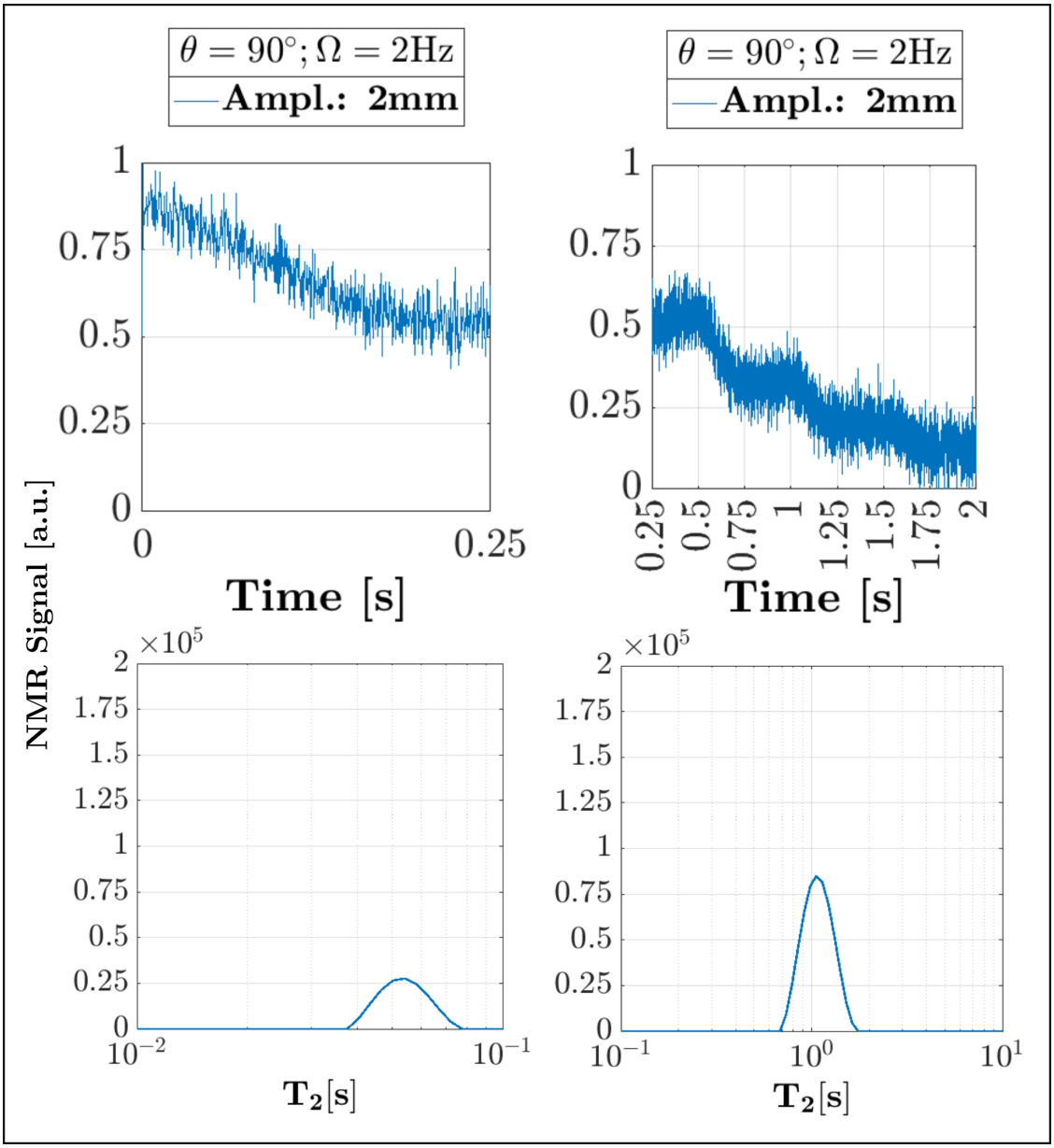

Figure 18 – As we can observe in the experimental results, there are two distinct components in the relaxation process. The faster component has a duration of approximately 0.25 s, which corresponds to half the oscillation period of the sample. This characteristic can be clearly seen in the experimental data. Source: By the author.

Moving forward, we aim to enhance our analysis by incorporating diffusion effects, taking our study to the next level. It is worth mentioning that the concepts presented here are still in their early stages of development.

4.5.3 Moving forward

Magnetic field inhomogeneity is a common issue in single-sided NMR that can cause resonance offsets across the sample, complicating conventional pulse sequences and reducing sensitivity during detection periods.[19–20] This section describes how the formation of echoes in the presence of a strong and uniform static gradient can be utilized to encode self-diffusion, which reveals molecular dynamics and sample microstructure.

Diffusion effects. When investigating the behavior of spins in an NMR experiment, one may take into account the effect of diffusion. This effect arises from the fact that the position of the spin experiences not only deterministic contributions due to oscillation but also stochastic contributions to its movement. In the case of molecular diffusion, these stochastic contributions are associated with the Brownian motion of molecules as they move in the presence of a non-homogeneous magnetic field.[48–50] The effect of diffusion on NMR signals is manifested as a phase shift relative to the refocusing pulses, which results in the nuclear spins failing to fully refocus. Consequently, the NMR signal observed is subject to additional attenuation, leading to a reduction in signal intensity.

The echo time, which represents the duration between the center of the radio frequency pulse and the center of the echo signal in a pulse sequence, can significantly impact the characteristics of the NMR signal observed. If the echo time is too short, the nuclear spins may not have sufficient time to fully evolve, leading to decreased signal intensity.[58] On the other hand, if the echo time is too long, the nuclear spins may experience diffusion processes that result in the loss of phase coherence. In unilateral low-field NMR sensors, the pulse sequence typically used is based on the generation of Hahn echo operating in the presence of a steady gradient (see Fig. 19) intensity.[58] To improve the sensitivity of these experiments, a CPMG sequence is applied after the so-called diffusion editing period ($t_{E,1}$) to generate an echo train that takes advantage of long transverse relaxation times of liquid samples. From now on, we will disregard the impact of relaxation on attenuation.

MOS-NMR and diffusion effects. Let's now examine NMR diffusion in porous media under LWD conditions, specifically with regard to oscillatory movements. With careful consideration of the relevant factors, the phase variable $\phi(z(t), t)$ is now a function that has the dependence of two terms, $\phi(z(t), t) = \phi_{\text{stochastic}}(t) + \phi_{\text{deterministic}}(t)$. The first one is related to diffusion movement and considers the position of the spin as a stochastic variable. The second, in turn, is related to the deterministic sinusoidal movement controlled by the experimenter.

The effects under study can be incorporated by accounting for the phase accumulation, which can be determined using the following approach

$$\Phi(z(t),t) = \gamma G_0 \int z_{\text{stochastic}}(t)\mathrm{d}t + \gamma G_0 \int z_{\text{deterministic}}(t)\mathrm{d}t. \tag{4.7}$$

Given the independence between the two phenomena under consideration, and in light of the information already presented in Section 4.4, the attenuation of the NMR signal can be described by the following equation

$$\overline{M}(2n\tau) = M(2n\tau)\exp\left(-i\phi_{\text{stochastic}}\right)_{2n}\exp\left(-i\phi_{\text{deterministic}}\right)_{2n}. \tag{4.8}$$

The presence of two distinct types of motion during the experiment becomes evident, each with its own distinct characteristics. Once again, it is worth noting that relaxation effects in our system result in a monoexponential decay, so incorporating these effects into our theoretical framework is relatively straightforward.

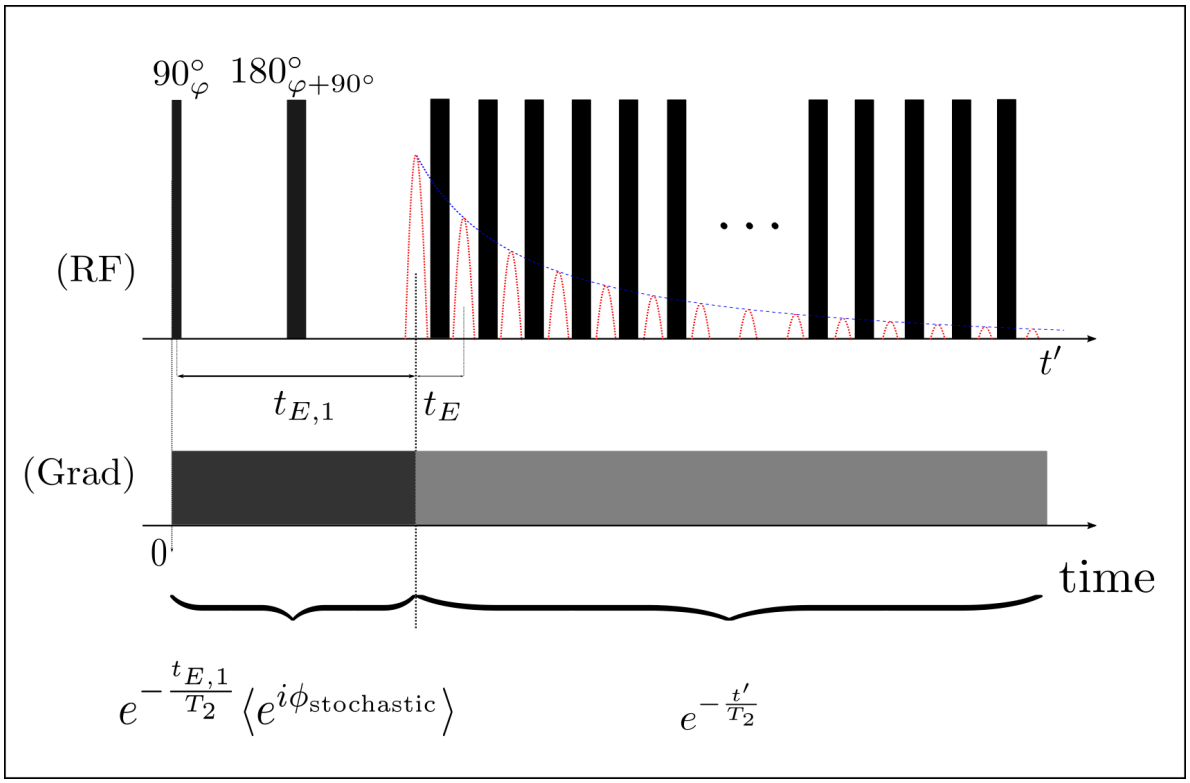

Figure 19 – This figure depicts pulse sequence utilized for diffusion editing, where Hahn echoes are generated in the presence of a static gradient. The first generated echo has an amplitude attenuated by diffusion.
Source: By the author.

Preliminary analysis. In the field of NMR in porous media, LWD conditions pose a unique challenge to diffusion measurements. These measurements are crucial in understanding the transport properties of fluids in porous media. Let us delve into some preliminary analysis of the effects on diffusion measurements in a CPMG experiment of NMR porous media under LWD conditions. It is crucial to first establish some foundational concepts. Understanding these concepts is essential to appreciate the significance of the key points and to gain insight into the complexities of the NMR diffusion measurements in porous media under LWD conditions.

- In a CPMG experiment, the diffusion coefficient of the fluid is related to the decay of the NMR signal, which is caused by the random motion of the fluid molecules in the presence of the applied gradient pulses. The diffusion coefficient can be estimated by fitting the signal decay to a model that describes the diffusion process.[70]

  The equation for the attenuation of the NMR signal in a CPMG experiment under the Gaussian regime and unrestricted diffusion is a simple and elegant expression[58]

  $$E = e^{-\frac{1}{2}\langle\Phi^2\rangle} = \frac{1}{12}\gamma^2 G_0^2 D t_{\mathrm{E}}^3, \tag{4.9}$$

  where D represents the diffusion coefficient. It describes the decay of the signal due to diffusion, and is given by a single exponential term in which the decay constant is proportional to the square of the diffusion coefficient and the square of the gradient strength.

- The traditional approach to measuring diffusion properties in NMR is based on the Gaussian regime. However, in the presence of strong gradients, this assumption may no longer hold true.[63–64]

  Furthermore, in the case of porous media, the diffusion regime may not need to be unrestricted. This is because porous media can contain complex pore geometries and heterogeneities. In unrestricted diffusion, the displacement of molecules is not confined by the pore size and shape, and instead reflects the underlying transport properties of the fluid.

- The effects of strong gradients on NMR measurements in porous media can be significant and complex. One primary effect is the dephasing of nuclear spins, which can lead to additional attenuation of the NMR signal. In addition, these spatial encoding effects can be especially problematic in the presence of oscillatory motions, where the coupling of the gradients with the motion can lead to additional attenuation and even more complex signal behavior.

Moreover, it is worth mentioning that when comparing the magnitudes of random movements in LWD acquisitions, such as molecular motion and tool-induced motion, the

latter overwhelmingly dominates the resulting attenuation. Therefore, considering this significant influence of tool-induced motion, the concept of regarding an LWD tool as a diffusion probe appears rather impractical.

4.6 Concluding remarks

To gain a deeper understanding of the intricate patterns observed in the NMR signal, we can simulate the operation of the LWD tool in standard temperature and pressure conditions while controlling specific movements with respect to the external magnetic field. This can be achieved by employing a mechanical system with a single-sided magnet and probes that replicate the sinusoidal motion between the external magnetic field and the sample. Through this approach, we can investigate the underlying mechanisms responsible for the observed patterns in the NMR signal.

The present manuscript focused on investigating the impacts caused by the variation of the amplitude at a fixed frequency, with the aim of simplifying the complexity of the problem as much as possible for just a few sets of parameters, so that this work, together with its results, can function as a *toy model*. It should be noted that the vast complexity of LWD conditions means that a complete and accurate description of real NMR measurements remains challenging, and this model can only serve as an introductory tool. With this in mind, it is possible to draw some preliminary conclusions.[42]

- We offer a comprehensive and introductory model that simulates the effect of oscillatory motion under the presence of a gradient magnetic field on the NMR signal, with the primary purpose of simulating LWD conditions. As an added benefit, interested readers have the ability to easily modify the parameters of this simulation to align with their unique objectives.

  It should be noted that the lack of accounting for *spatial RF selectivity* effects in the model at this stage does not necessarily mean that the observed outcomes are inaccurate. It simply means that there may be additional factors at play that could potentially affect the results. Moreover, through this exploration, it is hoped that a more nuanced understanding of the phenomenon under study will be achieved, ultimately contributing to the development of more comprehensive models that account for the complex dynamics of *spatial RF selectivity* effects.

- Our LWD simulator allows us to explore and distinguish the effects associated with the *spatial RF selectivity*. Even with just inverse Laplace technique analysis, we were able to separate the *two relaxation times* in the data presented in this manuscript.

  To rephrase, it can be said that we analyze all experimental data under the assumption of a monoexponential relaxation kernel, which may contradict earlier discussions about *spatial RF selectivity* effects and *phase modulation* in NMR signals, once they

might not exhibit the same decay signature as the physical intrinsic decay of the transverse relaxation time.

A critical aspect of our work that remains as a perspective is the development of a more refined data analysis to ensure the quality of the NMR signal, especially when dealing with complex conditions. This is of utmost importance in industrial applications, such as the oil and gas industry, where relaxation data play a vital role in estimating parameters like porosity and permeability. These parameters, in turn, serve as the basis for critical decision-making processes.

One simple processing technique that can potentially be used with the results presented in the current manuscript is performing the NMR signal inversion by introducing the calculated modulation factor within Equation (4.6) to assess the possibility of directly correcting the motion effect in the NMR processing.

Overall, this work presents experimental results obtained with our LWD simulator explained through the basic theoretical method employed. As a next step, we plan to study a set of representative rocks from the sandstone and carbonate families using the equipment presented in this manuscript. In addition, experiments related to the section discussing diffusion effects are already in progress. To minimize the effects associated with *spatial RF selectivity*, we aim to design more efficient probes that allow for the application of shorter RF pulses. Finally, we wholeheartedly encourage readers to engage with the LEAR group to offer any suggestions or report any errors, as we continually strive to refine and improve our methodologies.

5 CONCLUSIONS AND PERSPECTIVES

Reservoir and LWD conditions are characterized by intricate and demanding environments. The current state of the art in the field of NMR parameter estimation is continuously evolving to meet these challenges and continued research is needed to develop new techniques and methods for NMR measurements in porous media under these conditions.[42–46] In the present work, we were able to explore the impact of oscillatory motions on the measurements of NMR parameters, particularly the complexity of T_2 distributions.

The purpose of this work was to provide a concise yet comprehensive introduction to the theory of NMR relaxation and diffusion, as well as signal processing, and demonstrate their importance in the characterization of porous materials and their application in LWD conditions. The relaxation and diffusion properties of fluids in porous materials can provide valuable information about the pore structure, fluid dynamics, and fluid-solid interactions. Signal processing techniques, such as inversion algorithms, are essential for converting NMR signals into useful information about the sample. The conclusions drawn from this work are based on both the relevant literature and the author's own research, and are summarized in the following bullet points.[3−4,12−13,19−20]

- The low-field NMR technique and unilateral magnets have been long applied for the characterization of porous media. The positive sides of this technique include its ability to provide real-time measurements during drilling, allowing for more accurate and efficient characterization of subsurface formations. However, there are also some limitations to the technique, including the need for specialized equipment that can withstand the harsh conditions of drilling environments.

  While our work has focused on potential applications in the context of LWD tools, it is important to emphasize that depending on the drilling approach, different magnetic field profiles can be obtained. Thus, the suitability of the technique should be evaluated for each specific drilling environment, and the limitations of the technique must be considered when interpreting results.[19−20]

- CPMG pulse sequences in NMR have been widely used for the characterization of porous media, including applications in well-logging. In the presence of intricate environments, which are common in LWD conditions, advanced signal processing techniques may be applied to CPMG data to improve the accuracy of NMR parameter estimation and provide more detailed information about the pore structure of porous media. These techniques might be particularly useful in LWD-like conditions, where the signal-to-noise ratio may be lower and signal distortions may be more prevalent.

This master's work in NMR applied to porous media and conditions similar to LWD offers a plethora of exciting and promising research perspectives. The potential research directions are vast and varied, ranging from the development of novel pulse sequences and hardware to the exploration of fundamental aspects of NMR relaxation and diffusion mechanisms in porous media. Some possible perspectives are:[8–10,41–46,68]

- **Signal processing techniques.** Advanced signal processing techniques are necessary to extract useful information from the highly complex NMR signal in demanding environments. Signal processing techniques, such as machine learning algorithms, signal decomposition techniques, and advanced statistical analysis, may be utilized.
- **Combination with other characterization techniques.** NMR is frequently employed in conjunction with other characterization techniques such as X-ray microtomography (CT) or electron microscopy to acquire a more complete understanding of porous media.
- **Application to real-world problems.** The use of NMR as a tool for characterizing porous media offers numerous practical applications for solving real-world problems, particularly in the oil and gas industry. Its versatility make it an essential technique for studying porous media in different geological formations.

Despite these challenges, NMR remains a valuable tool for characterizing fluids and rocks in reservoirs and boreholes. Advances in hardware, software, and methodology continue to improve the accuracy and precision of NMR measurements under challenging conditions. These improvements will enable the continued use of NMR as a powerful tool for scientific research and practical applications.

The LEAR research group will face the challenge of sustaining their extensive research on the application of NMR to the study of porous media. The group has focused its efforts on this area, and their significant progress is evident in the development of novel methods for using unilateral NMR instruments to obtain information on fluid properties and reservoir properties.[41–42] This work has initiated the exploration of potential avenues for a deeper understanding of porous media and its potential implications for a variety of industries, making it a critical area of research for the LEAR group to pursue in future projects.

REFERENCES

1 INGHAM, D. B.; POP, I. **Transport phenomena in porous media**. Oxford: Elsevier, 1998.

2 ADLER, P. **Porous media**: geometry and transports. Oxford: Elsevier, 2013.

3 COATES, G.; XIAO, L.; PRAMMER, M. **NMR logging**: principles and applications. Houston: Haliburton Energy Services, 1999.

4 DUNN, K.-J.; BERGMAN, D. J.; LATORRACA, G. A. **Nuclear magnetic resonance**: petrophysical and logging applications. Amsterdam: Pergamon, 2002.

5 WATSON, A. T.; CHANG, C. P. Characterizing porous media with NMR methods. **Progress in Nuclear Magnetic Resonance Spectroscopy**, Elsevier, v. 31, n. 4, p. 343–386, 1997.

6 KLEINBERG, R. L. Nuclear magnetic resonance. **Experimental Methods in The Physical Sciences**, Elsevier, v. 35, p. 337–385, 1999.

7 BARRIE, P. J. Characterization of porous media using NMR methods. **Annual Reports on NMR Spectroscopy**, Academic Press, v. 41, p. 265–316, 2000.

8 SONG, Y.-Q. Focus on the physics of magnetic resonance on porous media. **New Journal of Physics**, IOP Publishing, v. 14, n. 5, p. 055017, 2012.

9 SONG, Y. *et al.* Magnetic resonance in porous media: recent progress. **Journal of Chemical Physics**, v. 128, n. 5, p. 02B618, 2008.

10 SONG, Y.-Q.; KAUSIK, R. NMR application in unconventional shale reservoirs–a new porous media research frontier. **Progress in Nuclear Magnetic Resonance Spectroscopy**, Elsevier, v. 112, p. 17–33, 2019.

11 ELSAYED, M. *et al.* A review on the applications of nuclear magnetic resonance (NMR) in the oil and gas industry: laboratory and field-scale measurements. **Journal of Petroleum Exploration and Production Technology**, Springer, v. 12, n. 10, p. 2747–2784, 2022.

12 MITCHELL, J. *et al.* Magnetic resonance imaging in laboratory petrophysical core analysis. **Physics Reports**, Elsevier, v. 526, n. 3, p. 165–225, 2013.

13 MITCHELL, J. *et al.* Low-field permanent magnets for industrial process and quality control. **Progress in Nuclear Magnetic Resonance Spectroscopy**, Elsevier, v. 76, p. 1–60, 2014.

14 KOSAREV, E. L. Applications of integral equations of the first kind in experiment physics. **Computer Physics Communications**, Elsevier, v. 20, n. 1, p. 69–75, 1980.

15 PROVENCHER, S. A constrained regularization method for inverting data represented by linear algebraic or integral equations. **Computer Physics Communications**, v. 27, n. 3, p. 213–227, 1982.

16 WHITTALL K.P.; MACKAY, A. Quantitative interpretation of NMR relaxation data. **Journal of Magnetic Resonance**, v. 84, n. 1, p. 134–152, 1989.

17 KLEINBERG, R. L. NMR measurement of petrophysical properties. **Concepts in Magnetic Resonance**, John Wiley & Sons, v. 13, n. 6, p. 404–406, 2001.

18 KLEINBERG, R. L. Well logging. *In*: **Encyclopedia of Nuclear Magnetic Resonance**. Chichester: Wiley, 1996. v. 8, p. 4960–4969.

19 BLÜMICH, B.; CASANOVA, F.; APPELT, S. NMR at low magnetic fields. **Chemical Physics Letters**, Elsevier, v. 477, n. 4-6, p. 231–240, 2009.

20 CASANOVA, F.; PERLO, J.; BLÜMICH, B. **Single-Sided NMR**. Berlin: Springer, 2011.

21 D'EURYDICE, M. **Desenvolvimento de metodologias para o estudo de meios porosos por Ressonância Magnética Nuclear**. 2011. Tese (Doutorado em Ciências) — Instituto de Física de São Carlos, Universidade de São Paulo, São Carlos, 2011.

22 MONTRAZI, E. T. **Estudo de cerâmicas porosas de alumina através da medida de tempos de relaxação via ressonância magnética nuclear**. 2012. Dissertação (Mestrado em Ciências) — Instituto de Física de São Carlos, Universidade de São Paulo, São Carlos, 2012.

23 LUCAS-OLIVEIRA, É. **Difusão de spins nucleares em meios porosos-uma abordagem computacional da RMN**. 2015. Dissertação (Mestrado em Ciências) — Instituto de Física de São Carlos, Universidade de São Paulo, São Carlos, 2015.

24 MONTRAZI, E. T. **Estudo da difusão de moléculas de fluidos em meios porosos por técnicas de Relaxation Exchange NMR**. 2016. Tese (Doutorado em Ciências) — Instituto de Física de São Carlos, Universidade de São Paulo, São Carlos, 2016.

25 TREVIZAN, W. A. **Nuclear magnetic resonance and digital rock in oil industry**: well logging applications. 2017. Tese (Doutorado em Ciências) — Instituto de Física de São Carlos, Universidade de São Paulo, São Carlos, 2017.

26 ANDREETA, M. B. **Topological study of reservoir rocks and acidification processes using complex networks methods**. 2017. Tese (Doutorado em Ciências) — Instituto de Física de São Carlos, Universidade de São Paulo, São Carlos, 2017.

27 OLIVEIRA, É. L. **Modelagem físico-computacional da RMN em meios porosos**: aplicações na indústria do petróleo. 2019. Tese (Doutorado em Ciências) — Instituto de Física de São Carlos, Universidade de São Paulo, São Carlos, 2019.

28 JÁCOMO, M. *et al.* Nuclear magnetic resonance characterization of porosity-preserving microcrystalline quartz coatings in fontainebleau sandstones. **Magnetic Resonance in Chemistry**, v. 39, n. 7, p. 406–408, 2001.

29 JÁCOMO, M. *et al.* Magnetic matrix nuclear magnetic resonance characterization of porosity-preserving microcrystalline quartz coatings in fontainebleau sandstones. **AAPG Bulletin**, v. 97, n. 11, p. 2117–2137, 2013.

30 D'EURYDICE, M. *et al.* T_2-filtered $T_2 - T_2$ exchange NMR. **Journal of Chemical Physics**, v. 144, n. 20, 2016.

31 LUCAS-OLIVEIRA, E. *et al.* Computational approach to integrate 3D x-ray microtomography and NMR data. **Journal of Magnetic Resonance**, v. 292, p. 16–24, 2018.

32 JÁCOMO, M. *et al.* Nuclear magnetic resonance and pore coupling in clay-coated sandstones with anomalous porosity preservation, ÿgua grande formation, recôncavo basin, brazil. **Petrophysics**, v. 59, n. 02, p. 136–152, 2018.

33 MONTRAZI, E. *et al.* Simultaneous acquisition for $T_2 - T_2$ exchange and $T_1 - T_2$ correlation NMR experiments. **Journal of Magnetic Resonance**, v. 289, p. 63–71, 2018.

34 BARSI-ANDREETA, M. *et al.* **Pore network and medial axis simultaneous extraction through maximal ball algorithm**. Available from: https://arxiv.org/abs/1912.04759. Acessible at: 27 February 2023.

35 MONTRAZI, E.; BONAGAMBA, T. Direct NMR T_1 distribution measurement without using ill-posed fitting methods. **Journal of Magnetic Resonance**, v. 309, p. 106624, 2019.

36 JÁCOMO, M. *et al.* Nuclear magnetic resonance characterization of porosity-preserving microcrystalline quartz coatings in fontainebleau sandstones. **AAPG Bulletin**, v. 103, n. 9, p. 2117–2137, 2019.

37 MONTRAZI, E.; BONAGAMBA, T. Saturation-recovery as a T_1-filter for T_2-T_2 exchange NMR. **Journal of Magnetic Resonance**, v. 301, p. 67–72, 2019.

38 LUCAS-OLIVEIRA, E. *et al.* Sandstone surface relaxivity determined by NMR T_2 distribution and digital rock simulation for permeability evaluation. **Journal of Petroleum Science and Engineering**, v. 193, p. 107400, 2020.

39 MONTRAZI, E. *et al.* New and rapid pulse sequences for two-dimensional $D - T_1$ correlation measurements. **Journal of Magnetic Resonance**, v. 315, p. 106749, 2020.

40 LUCAS-OLIVEIRA, E.; ARAÚJO-FERREIRA, A.; BONAGAMBA, T. Surface relaxivity probed by short-diffusion time NMR and digital rock NMR simulation. **Journal of Petroleum Science and Engineering**, v. 209, p. 107167, 2022.

41 OLIVEIRA-SILVA, R. de *et al.* A benchtop single-sided magnet with NMR well-logging tool specifications–examples of application. **Journal of Magnetic Resonance**, Elsevier, v. 322, p. 106871, 2021.

42 LUCAS-OLIVEIRA, E. *et al.* Mechanically oscillating sample under magnetic field gradients: MOS-NMR. **Journal of Magnetic Resonance Open**, v. 12-13, p. 100084, 2022.

43 COMAN, R. *et al.* Improved NMR logging approach to simultaneously determine porosity, T_2 and T_1. *In*: SPE Annual Technical Conference and Exhibition, 2015, Houston. **Abstract** [...] Houston: SPE, 2015. Paper number: SPE–175050–MS.

44 COMAN, R.; THERN, H.; KISCHKAT, T. Lateral-motion correction of NMR logging-while-drilling. *In*: SPWLA Annual Logging Symposium, 59th., 2018, London. **Abstract** [...] London: SPWLA, 2018. Paper number: SPWLA–2018–LLL.

45 O'NEILL, K. T. *et al.* Quantifying motional dynamics in nuclear magnetic resonance logging. **Journal of Magnetic Resonance**, Elsevier, v. 337, p. 107167, 2022.

46 SELBY, W.; GARLAND, P.; MASTIKHIN, I. Dynamic mechanical analysis with portable NMR. **Journal of Magnetic Resonance**, Elsevier, v. 339, p. 107211, 2022.

47 HÜRLIMANN, M. D.; HEATON, N. J. NMR Well Logging. *In*: Johns, M. L. *et al.* (ed.). **Mobile NMR and MRI:** developments and applications. Cambridge: Royal Society of Chemistry, 2015. p 11-85.

48 SLICHTER, C. **Principles of magnetic resonance**. Berlin: Springer, 1990.

49 ABRAGAM, A. **The principles of nuclear magnetism**. Oxford: Oxford University Press, 1961.

50 CALLAGHAN, P. **Principles of nuclear magnetic resonance microscopy**. Oxford: Oxford University Press on Demand, 1993.

51 BLOCH, F. Nuclear induction. **Physical Review**, v. 70, n. 7-8, p. 460–474, 1946.

52 PURCELL, E.; TORREY, H.; POUND, R. Resonance absorption by nuclear magnetic moments in a solid. **Physical Review**, v. 69, n. 1-2, p. 37–38, 1946.

53 CALLAGHAN, P. **Translational dynamics and magnetic resonance**: principles of pulsed gradient spin echo NMR. Oxford: Oxford University Press, 2011.

54 COWAN, B. **Nuclear magnetic resonance and relaxation**. New York: Cambridge University Press, 1997.

55 BLOEMBERGEN, N.; PURCELL, E.; POUND, R. Relaxation effects in nuclear magnetic resonance absorption. **Physical Review**, v. 73, n. 7, p. 679–712, 1948.

56 CARR, H.; PURCELL, E. Effects of diffusion on free precession in nuclear magnetic resonance experiments. **Physical Review**, v. 94, n. 3, p. 630–638, 1954.

57 MEIBOOM, S.; GILL, D. Modified spin-echo method for measuring nuclear relaxation times. **Review of Scientific Instruments**, v. 29, n. 8, p. 688–691, 1958.

58 HAHN, E. L. Spin echoes. **Physical Review**, v. 80, n. 4, p. 580–594, 1950.

59 PRICE, W. **NMR studies of translational motion**: principles and applications. Cambridge: Cambridge University Press, 2009.

60 GREBENKOV, D. NMR survey of reflected brownian motion. **Reviews of Modern Physics**, v. 79, n. 3, p. 1077–1137, 2007.

61 BROWNSTEIN, K.; TARR, C. Spin-lattice relaxation in a system governed by diffusion. **Journal of Magnetic Resonance**, v. 26, n. 1, p. 17–24, 1977.

62 BROWNSTEIN, K.; TARR, C. Importance of classical diffusion in NMR studies of water in biological cells. **Physical Review A**, v. 19, n. 6, p. 2446–2453, 1979.

63 GREBENKOV, D. S. Diffusion MRI/NMR at high gradients: challenges and perspectives. **Microporous and Mesoporous Materials**, Elsevier, v. 269, p. 79–82, 2018.

64 GREBENKOV, D. S. From the microstructure to diffusion NMR, and back. *In*: VALIULLIN, R. (ed.). **Diffusion NMR of Confined Systems:** fluid transport in porous solids and heterogeneous materials. Crydon: Royal Society of Chemistry, 2017. p 52-110.

65 HANSEN, P. **Discrete inverse problems**: insight and algorithms. Philadelphia: Society for Industrial and Applied Mathematics, 2010.

66 BARONE, P.; RAMPONI, A.; SEBASTIANI, G. On the numerical inversion of the laplace transform for nuclear magnetic resonance relaxometry. **Inverse Problems**, IOP Publishing, v. 17, n. 1, p. 77–94, 2001.

67 VENKATARAMANAN, L.; SONG, Y.; HURLIMANN, M. Solving fredholm integrals of the first kind with tensor product structure in 2 and 2.5 dimensions. **IEEE Transactions on Signal Processing**, v. 50, n. 5, p. 1017–1026, 2002.

68 CHEN, H. *et al.* A statistical learning perspective on the inversion of NMR relaxation data. **AIP Advances**, AIP Publishing LLC, v. 12, n. 6, p. 065230, 2022.

69 GIL, V. M.; GERALDES, C. F. G. C. **Ressonância magnética nuclear**: fundamentos, métodos e aplicações. Lisboa: Fundação Calouste Gulbenkian, 1987.

70 GREBENKOV, D. Use, misuse, and abuse of apparent diffusion coefficients. **Concepts in Magnetic Resonance**, v. 36, n. 1, p. 24–35, 2010.